IEEE Access
Multidisciplinary | Rapid Review | Open Access Journal

Received February 3, 2019, accepted February 24, 2019, date of publication February 27, 2019, date of current version March 20, 2019.

Digital Object Identifier 10.1109/ACCESS.2019.2901903

Quickly Obtaining Range of Articulated Rotating Speed for Electrically Driven Large-Load-Ratio Six-Legged Robot Based on Maximum Walking Speed Method

HONGCHAO ZHUANG[1], NING WANG[2], HAIBO GAO[3], AND ZONGQUAN DENG[3]

[1]College of Mechanical Engineering, Tianjin University of Technology and Education, Tianjin 300222, China
[2]College of Information Technology Engineering, Tianjin University of Technology and Education, Tianjin 300222, China
[3]State Key Laboratory of Robotics and System, Harbin Institute of Technology, Harbin 150001, China

Corresponding authors: Hongchao Zhuang (zhuanghongchao_hit@163.com) and Ning Wang (wangning811108@163.com)

This work was supported in part by the National Natural Science Foundation of China under Grant 51505335.

ABSTRACT The articulated rotating speed is one of the important parameters to determine the drive devices and actuating devices of joints for legged robots. Compared with the small-scale multi-legged robots, the range of the output speed of the joint should be as accurate as possible for the large-load-ratio multi-legged robots. To reasonably select the devices of joints, the maximum walking speed method is proposed to quickly and accurately obtain the range of articulated rotating speed by taking an electrically driven large-load-ratio six-legged robot as an example. To prove the rapidity, accuracy, and conciseness of the maximum walking speed method, the analyses of the forward kinematics and inverse kinematics of the robot are implemented based on the Denavit–Hartenberg method. However, only one range of articulated rotating speed is effectively confirmed in a single leg. Through rotating one of the joints to achieve the maximum speed index of the robot, the maximum walking speed method is employed to establish the mathematical relationships between the articulated rotating angles and the maximum walking speed index of the robot. The ranges of the output speeds of all joints are accurately obtained. The simulation verification and walking experiments of the prototype are, respectively, carried out. The results of the simulation and walking experiments show that the maximum walking speed method is reasonable and effective in calculating the range of articulated rotating speed. The proposed method in this paper can be reliably applied to the development of large-load-ratio multi-legged robots.

INDEX TERMS Large-load-ratio six-legged robot, articulated rotating speed, rotation angle, maximum walking speed method.

I. INTRODUCTION

At present, a large number of autonomous mobile robots are widely applied in people's daily work and life with the rapid development of robot technology [1]. Intelligence [2] and high trafficability [3], [4] are generally viewed as parts of the important development directions for the ground walking roots. According to the mobile modes of robots on the ground, the ground walking robots can be roughly divided into wheeled type, legged type, wheel-legged type, tracked type, and snaked type [5]. Meanwhile, wheeled and tracked robots move relatively fast, but their terrain adaptability is relatively weak. The legged and snaked robots have strong terrain transmission ability, but their moving speed is relatively low. The wheel-legged robots can take the advantages of both wheeled and legged robots into account, but they often have the complex structures and large mass. The snaked robots are the weakest in terms of load-carrying capacity. In view of the excellent terrain adaptability, carrying capacity, and wide use space, the legged robots have attracted the attention of many researchers. In the development of robots, the legged robots start relatively late in the aspects of the theoretical research and practical application, especially for the large-load-ratio multi-legged robots [6].

The associate editor coordinating the review of this manuscript and approving it for publication was Shafiqul Islam.

In the research of the multi-legged robots, many researchers often focus on gait planning [7], [8] and motion control [9]–[11]. Zhao *et al.* [12] proposed the obstacle avoidance and motion planning scheme for a hexapod robot. Mendez-Monroy [13] used a pattern generator to maintain the balance of humanoid robot in the presence of strong disturbance. Tian and Gao [14] provided an efficient motion planning method for a six-legged robot to traverse the terrain with medium irregularities. Martinez *et al.* [15] described a lower limb exoskeleton control approach for guiding leg movement. Xiong *et al.* [16] developed a neuromechanical controller consisting of a modular neural network and of virtual agonist-antagonist muscle mechanisms for a hexapod robot. Gor *et al.* [17] presented the quadruped locomotion control in the workspace through a novel control scheme.

Walking speed is one of the main technical indicators of a multi-legged robot. Based on the index of walking speed, there are relatively few papers on the analysis of articulated output speed for the legged robots. Many researchers mainly focus on other issues and do not spend much effort on the study of the walking speed of legged robots. Pratt and Tedrake [18] presented the velocity-based stability margins for fast bipedal walking. The simple models of walking such as an inverted pendulum model and the Linear Inverted Pendulum model were used to estimate the stability margins. Wang *et al.* [19] proposed a bio-inspired approach of velocity control for a quadruped robot running with a bounding gait on compliant legs. They built a velocity controller based on energy control and vestibular reflexes. Zhang *et al.* [20] optimized the distribution of joint torques and velocity of a redundant single leg with joint physical limitations. The modified optimization criterion combining joint torques with angular velocity was proposed. The methods for the velocity analysis of parallel robots generally include derivation method, screw method, vector method, tensor method, influence coefficient method, etc. [21] These methods often involve the solution of Jacobian matrix. The multi-legged robots are one kind of topological mechanisms, multi-link mechanisms and redundant underactuated mechanisms. Their kinematics and dynamics analyses are very complicated. Although the Jacobian matrix plays an important role in the research of robotics, it becomes more and more complicated with the increase of the robot degrees of freedom and brings a relatively large amount of calculation, which is not conducive to the development of the multi-legged robots.

According to the technical parameters of large-load-ratio multi-legged robots on ASV [22], BigDog [23], Ambler [24], Dante II [25], COMET-IV [26], and ATHLETE [3], we can conclude that the large-load-ratio multi-legged robots have three characteristics by comparing with the small-scale multi-legged robots; they are the larger size, bigger mass, and larger load ratio. The small-scale multi-legged robots basically do not have the capacity to carry materials. The relatively greater safety margin is caused because the articulated output speed is not the focus of attention for the small-scale multi-legged robots. In addition to carrying a variety of detection instruments in the outdoor environment to achieve scientific goals, the large-load-ratio multi-legged robots can also act as a transporter, which requires the robot to have the characteristics of the small mass and large bearing capacity. Hence, the range of the output speed of joint should be as accurate as possible for the large-load-ratio multi-legged robots, because the greater safety margin leads to the larger size and mass for the drive device and actuating device of joint. Then, the large-load-ratio multi-legged robots have the relatively low outdoor survivability and load ratio.

Although the D–H method can be used to carry out the analysis of articulated rotating speed, the large amount of calculation is caused. Based on the above problems, the maximum walking speed method is proposed to quickly and accurately obtain the articulated rotating speed by taking an electrically driven large-load-ratio six-legged robot as an example, which is conducive to providing data support for matching the drive devices and actuating devices of joints. To prove the rapidity, accuracy, and conciseness of the maximum walking speed method, the analyses of the forward kinematics and inverse kinematics of robot are also executed based on the D–H method in this article. This article is divided into seven sections. In Section 2, the configuration analysis is implemented for the electrically driven large-load-ratio six-legged robot. The body configuration and the linkage proportion of single leg are confirmed. In Section 3, the analyses of kinematics and inverse kinematics of the robot are carried out by the D–H method. The mathematical models are established for the articulated rotation angles of single leg. In Section 4, based on the rotation of a joint to achieve the maximum walking speed of robot, the maximum walking speed method is proposed. The mathematical relationships are established between the articulated rotation angles and the maximum walking speed of robot. The ranges of articulated output speeds are gained. In Section 5 the simulation analysis of walking is executed for the virtual prototype of robot. In Section 6, based on the development of electrically driven large-load-ratio six-legged robot, the walking experiments of prototype are performed. The rationality and validity of the maximum walking speed method are verified on the analysis of articulated rotating speed. In the final section, the conclusions are presented.

II. CONFIGURATION OF LARGE-LOAD-RATIO SIX-LEGGED ROBOT

To conveniently carry out the analysis of articulated rotating speed, the electrically driven large-load-ratio six-legged robot is called the large-load-ratio six-legged robot for short in this article. According to the structures of hexapod insects, we can know that most hexapod insects exhibit the elliptical projections on the ground, which is mainly determined by their own living environment. To prevent natural enemies or other organisms from disturbing, hexapod insects often live in ground or underground environments such as weeds, underground caves, leaves and branches crisscrossing each other. Hence, hexapod insects often have long structures along the

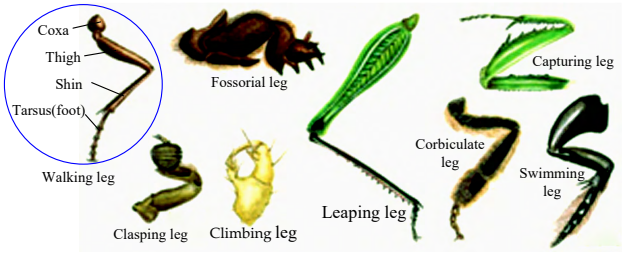

FIGURE 1. Structures of supporting legs for hexapod insects.

head-to-tail direction, narrow structures along the transverse direction, and symmetrically distributed legs on both sides of the body, which enables insects to have relatively high speed and stability. The supporting legs of hexapod insects have a variety of structures, generally including walking leg, leaping leg, clasping leg, fossorial leg, climbing leg, corbiculate leg, and so on; they are shown in Figure 1. The walking leg is the most basic and common type of thoracic legs in insects. And it is most suitable for walking because of its slender shape and no significant changes in its segments. In view of the characteristics of walking leg and the working environment of large-load-ratio six-legged robot, the robot configuration is designed according to the structures of walking leg.

The large-load-ratio six-legged robot is not a hexapod insect after all. And it can further improve its performance on the basis of the excellent characteristics of hexapod insects. The body configuration of large-load-ratio six-legged robot can be a circle or regular polygon, which makes the robot have the ability to walk in an omnidirectional direction and relatively high stability. Then, the performance of each leg can be exerted to realize the force distribution of foot and improve the load ratio of robot. The single leg of robot is designed based on the walking leg structure. Each leg contains three driving joints (abductor joint, hip joint, and knee joint), a passive spherical joint (ankle joint), and a passive straight joint (adaptive spring). Each leg has three linkages: a coxa, thigh, and shin. According to the structure of walking leg, we can conclude that the length of thigh is approximately equal with shin, and the length of coxa is the smallest. The axis of the abductor joint follows the direction of the $Z-$axis. The axes of the hip joint and knee joint run parallel to the direction of the $Y-$axis. Figure 2 illustrates the structure of single leg

In Figure 2, l_c, l_t, and l_s are respectively viewed as the lengths of coxa, thigh, and shin. The maximum obstacle height and maximum ditch width are respectively set as h_o and l_d. Figure 3 illustrates the scheme of length analysis for the shin. To guarantee the large-load-ratio six-legged robot on passing through the maximum obstacle and ditch and maintaining a certain body height, the length l_s of shin must be greater than the maximum obstacle height h_o and maximum ditch width l_d. Hence, the maximum obstacle height h_o of 1/3 is regarded as the height of safety compensation. Namely, the safety factor of maximum obstacle is about 1.3. According to Figure 3, we can obtain that the length l_s of shin

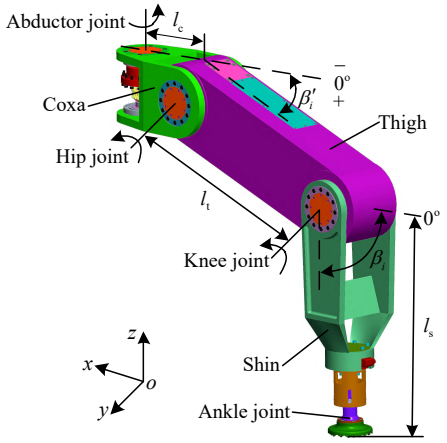

FIGURE 2. Structure of single leg of the electrically driven large-load-ratio six-legged robot.

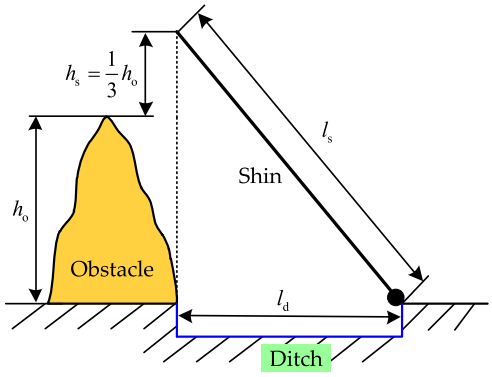

FIGURE 3. Scheme of length analysis of the shin.

is $\sqrt{16h_o^2/9 + l_d^2}$. The length of robot's coxa is restricted by the sizes of drive devices and actuating devices at the abductor joint and hip joint, so it cannot be as small as the coxa of hexapod insect. Based on the outer envelope dimension index of the large-load-ratio six-legged robot, the linkage proportion of single leg is set as 9: 25: 25 for the lengths of coxa, thigh, and shin.

To maintain the characteristics of universal walking, the configuration of body is designed as a regular polygon for the large-load-ratio six-legged robot. Figure 4 illustrates the mechanism diagram of large-load- ratio six-legged robot. In Figure 4, The abductor joint, hip joint, and knee joint are respectively defined as A_i, H_i, and $K_i(i = 1–6)$. o_i and r_{bp} represent the foothold of leg i and the distance between abductor joint and center of body. $\sum_B (O_B - X_B Y_B Z_B)$ and $\sum_G (O_G - X_G Y_G Z_G)$ are respectively regarded as the body coordinate system located at the center of body and the ground coordinate system. The coordinate systems of abductor joint A_i, hip joint H_i, and knee joint K_i of the leg i are defined as $\sum_{A_i}\left(A_i - x_1^{(i)} y_1^{(i)} z_1^{(i)}\right)$, $\sum_{H_i}\left(H_i - x_2^{(i)} y_2^{(i)} z_2^{(i)}\right)$, and $\sum_{K_i}\left(K_i - x_3^{(i)} y_3^{(i)} z_3^{(i)}\right)$ respectively. The $x_1^{(i)}$-axis is parallel to the coxa of leg i. The $z_1^{(i)}$ -axis is kept parallel with the

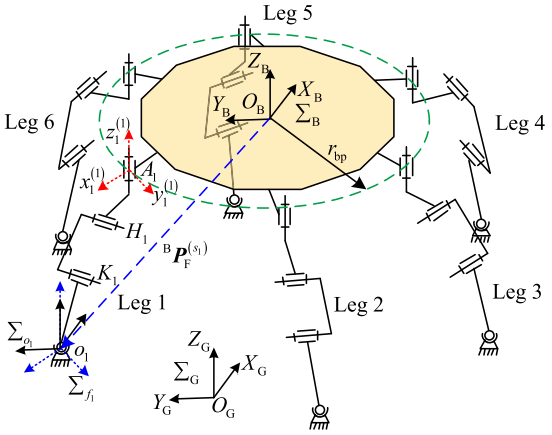

FIGURE 4. Mechanism diagram of the electrically driven large-load- ratio six-legged robot.

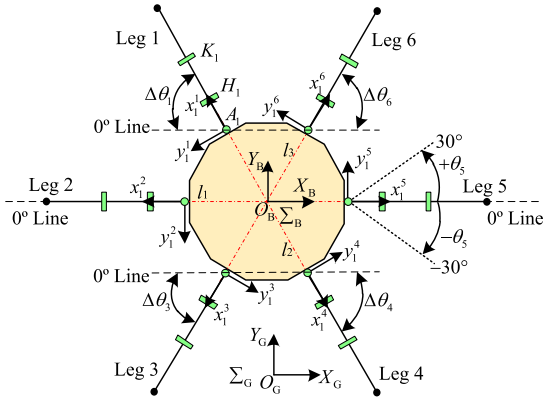

FIGURE 5. Top view of the mechanism of the electrically driven large-load-ratio six-legged robot.

Z_B-axis of body coordinate system $\sum_B$. The foot coordinate system $\sum_{o_i}$ and the body coordinate system $\sum_B$ are parallel to each other for the leg i. The foot coordinate system $\sum_{f_i}$ is parallel to the coordinate system $\sum_{A_i}$ of abductor joint for the leg i. ${}^{B}\boldsymbol{P}_{F}^{(s_k)}$ represents the foot position matrix of leg s_k in the body coordinate system $\sum_B$. The large-load-ratio six-legged robot is a 6-RRRS series mechanism.

III. KINEMATIC ANALYSIS OF LARGE-LOAD-RATIO SIX-LEGGED ROBOT

A. ESTABLISHMENT OF ROBOT D-H MODEL

Figure 5 illustrates the top view of mechanism for the large-load-ratio six-legged robot. In Figure 5, the 0° lines are parallel to the X_B-axis of the Σ_B and pass through the origins of the coordinate systems of abductor joints. The included angle $\Delta\theta_i$ between 0° line and leg i, which is used to set the initial position of abductor joint when the robot begins to walk, is defined as the initial angle of abductor joint. The included angle $\Delta\theta_i$ ranges from 0° to 60°. Based on the initial angle $\Delta\theta_i$, θ_i is regarded as the rotation angle of abductor joint. The initial angles $\Delta\theta_2$ of leg 2 and $\Delta\theta_5$ of leg 5 are always zero degrees. The initial angles $\Delta\theta_1$ of leg 1, $\Delta\theta_3$ of leg 3, $\Delta\theta_4$ of leg 4, and $\Delta\theta_6$ of leg 6 can vary within

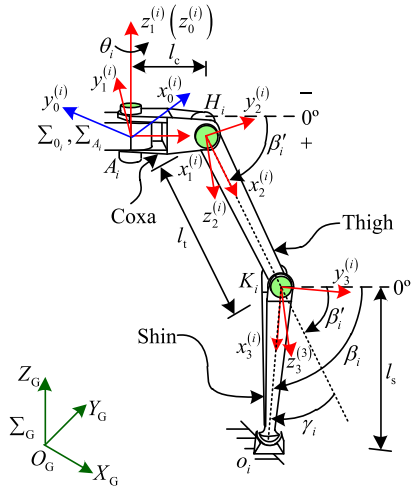

FIGURE 6. D-H model of leg i of the electrically driven large-load-ratio six-legged robot.

their interval, and they are equal to each other when the robot begins to walk.

Figure 6 illustrates the D-H model of leg i. In Figure 6, β_i' is regarded as the rotation angle between the coxa of leg i and the thigh of leg i γ_i is regarded as the rotation angle between the thigh of leg i and the shin of leg i. The rotation angle between the coxa of leg i and the shin of leg i is defined as β_i. Then, the relation can be obtained among β_i', γ_i, and β_i; it is $\beta_i = \beta_i' + \gamma_i$. H represents the distance from the body centroid O_B to the ground. h_i is viewed as the distance from the origin of coordinate system of the abductor joint A_i to the ground. We can gain that the relation is $h_i = H$. The $z_1^{(i)}$-axes of the abductor joints are kept parallel with the Z_G-axis when the body bottom is parallel to the ground. The $y_1^{(i)}$-axis is parallel to the rotation axes of the hip joint and knee joint of the leg i.

The range of θ_i is from 0° to 60°. To avoid the interferences caused by the articulated rotation, the effective intervals of θ_i, β_i', and β_i can be obtained through plotting the rotation amplitudes of joints under the coordinate system of abductor joint A_i of the leg i; they are from −30° to 30° for θ_i, from −90° to 90° for β_i', and from 0° to 150° for β_i. The positive and negative values of angles are related to the positive and negative directions of the prescribed rotation of joint. The articulated torques of leg i are only related to the foot force and the arm of force. When the angle of knee joint is fixed, the hip joint has the same force arm at $-\beta_i'$ and $+\beta_i'$. To analyze conveniently and obtain effective articulated rotating speed, the theoretical analysis of the rotating speed of joint is carried out under the constraint condition $(0° \le \beta_i' \le \beta_i \le 90°)$.

According to the D-H method presented by Craig [27], the D-H kinematics model of leg i is established. The parameters of the D-H model of leg i are shown in Table 1. Based on the rules of D-H method, the coordinate system $\sum_{0_i}\left(0_i - x_0^{(i)} y_0^{(i)} z_0^{(i)}\right)$ locates at the body and connects the

TABLE 1. Parameters of the D-H model of leg *i*.

Joint j	Linkage Length $a_{j-1}^{(i)}$ (mm)	Torsion Angle of Linkage $\alpha_{j-1}^{(i)}$ (deg)	Linkage Offset $d_j^{(i)}$ (mm)	Rotation Angle of Linkage $\theta_j^{(i)}$ (deg)
1	0	0°	0	θ_i
2	l_c	90°	0	β_i'
3	l_t	0°	0	γ_i

body to the leg i. The coordinate system $\sum_{0_i}$ and coordinate system $\sum_{A_i}$ are coincident with each other when the rotating angle θ_i of the abductor joint is the value of zero degrees.

B. FORWARD KINEMATICS ANALYSIS OF THE LARGE-LOAD-RATIO SIX-LEGGED ROBOT

The foot position of each leg of the large-load-ratio six-legged robot is solved with the known body postures and articulated rotating angles under the ground coordinate system. The analysis of the forward kinematics can be performed. Based on Figure 6, the mathematical relation can be obtained. Then

$$\beta_i = \beta_i{}' + \gamma_i \tag{1}$$

The transformation matrix ${}_{j}^{j-1}\boldsymbol{T}^{(i)}$ between the joint $(j-1)$ and joint j of leg i can be expressed as follows. Then (2), as shown at the bottom of this page.

The parameters of the D-H model of leg i in Table 1 are brought into (2). The transformation matrixes of joint coordinates can be written among the joints of leg i. Then

$${}_{1}^{0}\boldsymbol{T}^{(i)} = \begin{pmatrix} \cos\theta_i & -\sin\theta_i & 0 & 0 \\ \sin\theta_i & \cos\theta_i & 0 & 0 \\ 0 & 0 & 1 & 0 \\ 0 & 0 & 0 & 1 \end{pmatrix} \tag{3}$$

$${}_{2}^{1}\boldsymbol{T}^{(i)} = \begin{pmatrix} \cos\beta'_i & -\sin\beta'_i & 0 & l_c \\ 0 & 0 & -1 & 0 \\ \sin\beta'_i & \cos\beta'_i & 0 & 0 \\ 0 & 0 & 0 & 1 \end{pmatrix} \tag{4}$$

$${}_{3}^{2}\boldsymbol{T}^{(i)} = \begin{pmatrix} \cos\gamma_i & -\sin\gamma_i & 0 & l_t \\ \sin\gamma_i & \cos\gamma_i & 0 & 0 \\ 0 & 0 & 1 & 0 \\ 0 & 0 & 0 & 1 \end{pmatrix} \tag{5}$$

Based on (3), (4), and (5), the transformation matrix ${}_{3}^{0}\boldsymbol{T}^{(i)}$ from the coordinate system $\sum_{K_i}$ to the coordinate system $\sum_{0_i}$ can be written for the leg i (6), as shown at the bottom of this page.

The coordinate matrix of foot end of the leg i can be written under the coordinate system $\sum_{K_i}$ of knee joint. Then

$${}^{3}\boldsymbol{P}_{\mathrm{F}}^{(i)} = \begin{pmatrix} l_s \\ 0 \\ 0 \\ 1 \end{pmatrix} \tag{7}$$

The transformation matrix ${}_{0}^{\mathrm{B}}\boldsymbol{T}^{(i)}$ from the coordinate system $\sum_{0_i}$ to the coordinate system $\sum_{\mathrm{B}}$ of body can then be written as follows. Then

$${}_{0}^{\mathrm{B}}\boldsymbol{T}^{(i)} = \begin{pmatrix} {}_{0}^{\mathrm{B}}\boldsymbol{R}^{(i)} & {}^{\mathrm{B}}\boldsymbol{P}_{0}^{(i)} \\ \boldsymbol{O} & 1 \end{pmatrix} \in \boldsymbol{R}^{4\times4} \tag{8}$$

where ${}_{0}^{\mathrm{B}}\boldsymbol{R}^{(i)}$ is the rotation matrix from the coordinate system $\sum_{0_i}$ to the coordinate system $\sum_{\mathrm{B}}$ of body, ${}_{0}^{\mathrm{B}}\boldsymbol{R}^{(i)} \in \boldsymbol{R}^{3\times3}$. ${}^{\mathrm{B}}\boldsymbol{P}_{0}^{(i)}$ is the position matrix from the coordinate system $\sum_{0_i}$ to the coordinate system $\sum_{\mathrm{B}}$ of body, ${}^{\mathrm{B}}\boldsymbol{P}_{0}^{(i)} \in \boldsymbol{R}^{3\times1}$. $\boldsymbol{O}$ is the zero matrix.

Based on Figure 5, Φ_i is regarded as the rotation angle between the coordinate system $\sum_{0_i}$ and the coordinate system $\sum_{\mathrm{B}}$ for the leg i. Hence, the values of rotation angle Φ_i are respectively set to 120°, 180°, 240°, 300°, 360°, and 60° for legs 1, 2, 3, 4, 5, and 6. The rotation matrix and position matrix can then be written as follows. Then

$${}_{0}^{\mathrm{B}}\boldsymbol{R}^{(i)} = \begin{pmatrix} \cos\Phi_i & -\sin\Phi_i & 0 \\ \sin\Phi_i & \cos\Phi_i & 0 \\ 0 & 0 & 1 \end{pmatrix} \tag{9}$$

$${}^{\mathrm{B}}\boldsymbol{P}_{0}^{(i)} = \begin{pmatrix} {}^{\mathrm{B}}\boldsymbol{P}_{0x}^{(i)} \\ {}^{\mathrm{B}}\boldsymbol{P}_{0y}^{(i)} \\ {}^{\mathrm{B}}\boldsymbol{P}_{0z}^{(i)} \end{pmatrix} \tag{10}$$

$${}_{j}^{j-1}\boldsymbol{T}^{(i)} = \begin{pmatrix} \cos\theta_j^{(i)} & -\sin\theta_j^{(i)} & 0 & a_{j-1}^{(i)} \\ \sin\theta_j^{(i)}\cos\alpha_{j-1}^{(i)} & \cos\theta_j^{(i)}\cos\alpha_{j-1}^{(i)} & -\sin\alpha_{j-1}^{(i)} & -d_j^{(i)}\sin\alpha_{j-1}^{(i)} \\ \sin\theta_j^{(i)}\sin\alpha_{j-1}^{(i)} & \cos\theta_j^{(i)}\sin\alpha_{j-1}^{(i)} & \cos\alpha_{j-1}^{(i)} & d_j^{(i)}\cos\alpha_{j-1}^{(i)} \\ 0 & 0 & 0 & 1 \end{pmatrix} \tag{2}$$

$${}_{3}^{0}\boldsymbol{T}^{(i)} = \begin{pmatrix} \cos\theta_i\cos\beta_i & -\cos\theta_i\sin\beta_i & \sin\theta_i & l_t\cos\theta_i\cos\beta'_i + l_c\cos\theta_i \\ \sin\theta_i\cos\beta_i & -\sin\theta_i\sin\beta_i & -\cos\theta_i & l_t\sin\theta_i\cos\beta'_i + l_c\sin\theta_i \\ \sin\beta_i & \cos\beta_i & 0 & l_t\sin\beta'_i \\ 0 & 0 & 0 & 1 \end{pmatrix} \tag{6}$$

The foot position matrix ${}^{\mathrm{B}}\boldsymbol{P}_{\mathrm{F}}^{(i)}$ of leg i can be written under the coordinate system $\sum_{\mathrm{B}}$ of body. Then

$$
\begin{aligned}
{}^{\mathrm{B}}\boldsymbol{P}_{\mathrm{F}}^{(i)} &= {}_{0}^{\mathrm{B}}\boldsymbol{T}^{(i)}{}_{3}^{0}\boldsymbol{T}^{(i)}{}^{3}\boldsymbol{P}_{\mathrm{F}}^{(i)} \\
&= \begin{pmatrix} \cos\left(\Phi_i+\theta_i\right)\left(l_{\mathrm{s}}\cos\beta_i + l_{\mathrm{t}}\cos\beta'_i + l_{\mathrm{c}}\right) + {}^{\mathrm{B}}\boldsymbol{P}_{0x}^{(i)} \\ \sin\left(\Phi_i+\theta_i\right)\left(l_{\mathrm{s}}\cos\beta_i + l_{\mathrm{t}}\cos\beta'_i + l_{\mathrm{c}}\right) + {}^{\mathrm{B}}\boldsymbol{P}_{0y}^{(i)} \\ l_{\mathrm{s}}\sin\beta_i + l_{\mathrm{t}}\sin\beta'_i + {}^{\mathrm{B}}\boldsymbol{P}_{0z}^{(i)} \\ 1 \end{pmatrix}
\end{aligned} \tag{11}
$$

The $Z-$axes of coordinate systems of the hip joint and knee joint are positively opposite to that specified in Figure 6, when the torsion angle $\alpha_{j-1}^{(i)}$ of linkage is changed from 90° to −90° for the hip joint of leg i. The foot position matrix ${}^{\mathrm{B}}\boldsymbol{P}_{\mathrm{F}}^{(i)}$ of leg i can be regained under the coordinate system $\sum_{\mathrm{B}}$ of body. Then

$$
\begin{aligned}
&{}^{\mathrm{B}}\boldsymbol{P}_{\mathrm{F}}^{(i)} \\
&= {}_{0}^{\mathrm{B}}\boldsymbol{T}^{(i)}{}_{3}^{0}\boldsymbol{T}^{(i)}{}^{3}\boldsymbol{P}_{\mathrm{F}}^{(i)} \\
&= \begin{pmatrix} \cos\left(\Phi_i+\theta_i\right)\left(l_{\mathrm{s}}\cos\beta_i + l_{\mathrm{t}}\cos\beta'_i + l_{\mathrm{c}}\right) + {}^{\mathrm{B}}\boldsymbol{P}_{0x}^{(i)} \\ \sin\left(\Phi_i+\theta_i\right)\left(l_{\mathrm{s}}\cos\beta_i + l_{\mathrm{t}}\cos\beta'_i + l_{\mathrm{c}}\right) + {}^{\mathrm{B}}\boldsymbol{P}_{0y}^{(i)} \\ -l_{\mathrm{s}}\sin\beta_i - l_{\mathrm{t}}\sin\beta'_i + {}^{\mathrm{B}}\boldsymbol{P}_{0z}^{(i)} \\ 1 \end{pmatrix}
\end{aligned} \tag{12}
$$

Based on (11) and (12), we can conclude that the $Z-$axis forward selection of the hip joint coordinate system $\sum_{H_i}$ only affects the Z directional position vector sign of foot end of the leg i under the coordinate system $\sum_{0_i}$. Hence, The results of (11) and (12) are correct. Then, the forward and inverse kinematics analyses are carried out based on (11).

When the articulated rotation angles have been gained for the abductor joint, hip joint, and knee joint of leg i, the mathematical expressions can be written for the position components of the foot in the directions of x, y, and z. Then

$$
{}^{\mathrm{B}}P_{\mathrm{F}x}^{(i)} = \cos\left(\Phi_i+\theta_i\right)\left(l_{\mathrm{s}}\cos\beta_i + l_{\mathrm{t}}\cos\beta'_i + l_{\mathrm{c}}\right) + {}^{\mathrm{B}}P_{0x}^{(i)} \tag{13}
$$

$$
{}^{\mathrm{B}}P_{\mathrm{F}y}^{(i)} = \sin\left(\Phi_i+\theta_i\right)\left(l_{\mathrm{s}}\cos\beta_i + l_{\mathrm{t}}\cos\beta'_i + l_{\mathrm{c}}\right) + {}^{\mathrm{B}}P_{0y}^{(i)} \tag{14}
$$

$$
{}^{\mathrm{B}}P_{\mathrm{F}z}^{(i)} = l_{\mathrm{s}}\sin\beta_i + l_{\mathrm{t}}\sin\beta'_i + {}^{\mathrm{B}}P_{0z}^{(i)} \tag{15}
$$

According to the ground coordinate system Σ_{G}, the position matrix ${}^{\mathrm{G}}\boldsymbol{P}_{\mathrm{F}}^{(i)}$ of the foot of leg i can then be expressed as follows. Then

$$
{}^{\mathrm{G}}\boldsymbol{P}_{\mathrm{F}}^{(i)} = {}_{\mathrm{B}}^{\mathrm{G}}\boldsymbol{T}^{(i)}{}^{\mathrm{B}}\boldsymbol{P}_{\mathrm{F}}^{(i)} = \begin{pmatrix} {}_{\mathrm{B}}^{\mathrm{G}}\boldsymbol{R}^{(i)} & {}^{\mathrm{G}}\boldsymbol{P}_{\mathrm{B}}^{(i)} \\ \boldsymbol{O} & 1 \end{pmatrix} \begin{pmatrix} {}^{\mathrm{B}}\boldsymbol{P}_{\mathrm{F}x}^{(i)} \\ {}^{\mathrm{B}}\boldsymbol{P}_{\mathrm{F}y}^{(i)} \\ {}^{\mathrm{B}}\boldsymbol{P}_{\mathrm{F}z}^{(i)} \\ 1 \end{pmatrix} \tag{16}
$$

where ${}_{\mathrm{B}}^{\mathrm{G}}\boldsymbol{T}^{(i)}$ is the transformation matrix from the body coordinate system $\sum_{\mathrm{B}}$ to the ground coordinate system $\sum_{\mathrm{G}}$, ${}_{\mathrm{B}}^{\mathrm{G}}\boldsymbol{T}^{(i)} \in \boldsymbol{R}^{4\times4}$. ${}_{\mathrm{B}}^{\mathrm{G}}\boldsymbol{R}^{(i)}$ is the rotation matrix from the body coordinate system $\sum_{\mathrm{B}}$ of body to the ground coordinate system $\sum_{\mathrm{G}}$, ${}_{\mathrm{B}}^{\mathrm{G}}\boldsymbol{R}^{(i)} \in \boldsymbol{R}^{3\times3}$. ${}^{\mathrm{G}}\boldsymbol{P}_{\mathrm{B}}^{(i)}$ is the translation matrix from the body coordinate system $\sum_{\mathrm{B}}$ to the ground coordinate system $\sum_{\mathrm{G}}$, ${}^{\mathrm{G}}\boldsymbol{P}_{\mathrm{B}}^{(i)} \in \boldsymbol{R}^{3\times1}$.

C. CINVERSE KINEMATICS ANALYSIS OF THE LARGE-LOAD-RATIO SIX-LEGGED ROBOT

The walking of robot is realized by controlling the driving joints of legs in the support phase and transfer phase, which refers to the inverse kinematics calculation of the robot. When the support phase contains u legs, an u–RRRS parallel platform with six degrees of freedom is comprised of the body of robot, ground, and u legs. The number of supporting legs should meet $3 \le u \le 6$ under the static gait. The rotation angles of the driving joints of each leg can be calculated when the foot trajectories of the support phase and transfer phase are known in Cartesian space. Figure 7 illustrates the posture of leg i for the large-load-ratio six-legged robot.

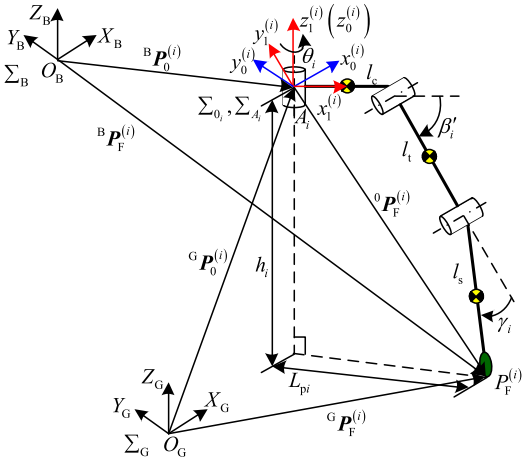

FIGURE 7. Posture of leg *i* of the large-load-ratio six-legged robot.

In Figure 7, $L_{\mathrm{p}i}$ is the projection length of the leg i in the coordinate system $\sum_{A_i}$ of the abductor joint, and it is called the span in this article. Based on Figure 7, the position matrix ${}^{\mathrm{G}}\boldsymbol{P}_{\mathrm{F}}^{(i)}$ from the foot of leg i to the coordinate system $\sum_{\mathrm{G}}$ of the ground can be written. Then

$$
{}^{\mathrm{G}}\boldsymbol{P}_{\mathrm{F}}^{(i)} = {}^{\mathrm{G}}\boldsymbol{P}_{0}^{(i)} + {}^{0}\boldsymbol{P}_{\mathrm{F}}^{(i)} = {}_{\mathrm{B}}^{\mathrm{G}}\boldsymbol{T}^{(i)}{}^{\mathrm{B}}\boldsymbol{P}_{0}^{(i)} + {}^{0}\boldsymbol{P}_{\mathrm{F}}^{(i)} \tag{17}
$$

where ${}^{\mathrm{G}}\boldsymbol{P}_{0}^{(i)}$ is the position matrix from the coordinate system $\sum_{0_i}$ to the coordinate system $\sum_{\mathrm{G}}$ of the ground, ${}^{\mathrm{G}}\boldsymbol{P}_{0}^{(i)} = {}_{\mathrm{B}}^{\mathrm{G}}\boldsymbol{T}^{(i)}{}^{\mathrm{B}}\boldsymbol{P}_{0}^{(i)}$. ${}^{0}\boldsymbol{P}_{\mathrm{F}}^{(i)}$ is the position matrix of the foot of leg i in the coordinate system $\sum_{0_i}$.

Based on (17), the position matrix ${}^{0}\boldsymbol{P}_{\mathrm{F}}^{(i)}$ can be obtained as follows. Then

$$
{}^{0}\boldsymbol{P}_{\mathrm{F}}^{(i)} = {}^{\mathrm{G}}\boldsymbol{P}_{\mathrm{F}}^{(i)} - {}_{\mathrm{B}}^{\mathrm{G}}\boldsymbol{T}^{(i)}{}^{\mathrm{B}}\boldsymbol{P}_{0}^{(i)} \tag{18}
$$

The position matrix ${}^{\mathrm{G}}\boldsymbol{P}_{\mathrm{F}}^{(i)}$ of the foot can be obtained when the foot trajectory of leg i has been determined in the gait period. Based on (18), the position matrix ${}^{0}\boldsymbol{P}_{\mathrm{F}}^{(i)}$ of foot end of the leg i can be gained under the coordinate system $\sum_{0_i}$. Hence, the rotation angles of the leg i are solved for the

abductor joint, hip joint, and knee joint, when the position matrix ${}^{0}\boldsymbol{P}_{\mathrm{F}}^{(i)}$ has been acquired. According to (13) and (14), the mathematical expressions are written as follows. Meanwhile, the rotation angle θ_i of abductor joint can be obtained. Then

$$\frac{{}^{\mathrm{B}}P_{\mathrm{F}x}^{(i)} - {}^{\mathrm{B}}P_{0x}^{(i)}}{\cos\left(\Phi_i + \theta_i\right)} = \frac{{}^{\mathrm{B}}P_{\mathrm{F}y}^{(i)} - {}^{\mathrm{B}}P_{0y}^{(i)}}{\sin\left(\Phi_i + \theta_i\right)} \tag{19}$$

$$\theta_i = \arctan\left(\frac{{}^{\mathrm{B}}P_{\mathrm{F}y}^{(i)} - {}^{\mathrm{B}}P_{0y}^{(i)}}{{}^{\mathrm{B}}P_{\mathrm{F}x}^{(i)} - {}^{\mathrm{B}}P_{0x}^{(i)}}\right) - \Phi_i \tag{20}$$

${}^{\mathrm{B}}P_{0x}^{(i)}$ and ${}^{\mathrm{B}}P_{0y}^{(i)}$ are respectively moved to the left sides of (13) and (14). Then the squares of the two equations are taken respectively. And the two equations are added together. The mathematical expression can be obtained. Then

$$\left({}^{\mathrm{B}}P_{\mathrm{F}x}^{(i)} - {}^{\mathrm{B}}P_{0x}^{(i)}\right)^2 + \left({}^{\mathrm{B}}P_{\mathrm{F}y}^{(i)} - {}^{\mathrm{B}}P_{0y}^{(i)}\right)^2 = \left(l_{\mathrm{s}}\cos\beta_i + \left(l_{\mathrm{t}}\cos{\beta'}_i + l_{\mathrm{c}}\right)\right)^2 \tag{21}$$

The extraction of square root and formula transformation are actualized for (21). The mathematical expression can be written. Then

$$\sqrt{\left({}^{\mathrm{B}}P_{\mathrm{F}x}^{(i)} - {}^{\mathrm{B}}P_{0x}^{(i)}\right)^2 + \left({}^{\mathrm{B}}P_{\mathrm{F}y}^{(i)} - {}^{\mathrm{B}}P_{0y}^{(i)}\right)^2} - l_{\mathrm{c}} = l_{\mathrm{s}}\cos\beta_i + l_{\mathrm{t}}\cos{\beta'}_i \tag{22}$$

The square on both sides of (22) is executed. Equation (23) can be obtained. Then

$$\left(\sqrt{\left({}^{\mathrm{B}}P_{\mathrm{F}x}^{(i)} - {}^{\mathrm{B}}P_{0x}^{(i)}\right)^2 + \left({}^{\mathrm{B}}P_{\mathrm{F}y}^{(i)} - {}^{\mathrm{B}}P_{0y}^{(i)}\right)^2} - l_{\mathrm{c}}\right)^2 = \left(l_{\mathrm{s}}\cos\beta_i + l_{\mathrm{t}}\cos{\beta'}_i\right)^2 \tag{23}$$

${}^{\mathrm{B}}P_{0z}^{(i)}$ in (15) is moved to the left side of equation. The squares are executed simultaneously on both sides of equation. The mathematical expression can be gained. Then

$$\left({}^{\mathrm{B}}P_{\mathrm{F}z}^{(i)} - {}^{\mathrm{B}}P_{0z}^{(i)}\right)^2 = \left(l_{\mathrm{s}}\sin\beta_i + l_{\mathrm{t}}\sin{\beta'}_i\right)^2 \tag{24}$$

Equation (23) adds (24) together. Equation (25) can be obtained. Then

$$\left(\sqrt{\left({}^{\mathrm{B}}P_{\mathrm{F}x}^{(i)} - {}^{\mathrm{B}}P_{0x}^{(i)}\right)^2 + \left({}^{\mathrm{B}}P_{\mathrm{F}y}^{(i)} - {}^{\mathrm{B}}P_{0y}^{(i)}\right)^2} - l_{\mathrm{c}}\right)^2 + \left({}^{\mathrm{B}}P_{\mathrm{F}z}^{(i)} - {}^{\mathrm{B}}P_{0z}^{(i)}\right)^2 = l_{\mathrm{s}}^2 + l_{\mathrm{t}}^2 + 2l_{\mathrm{s}}l_{\mathrm{t}}\cos\gamma_i \tag{25}$$

Based on (25), the rotation angle γ_i of knee joint can be obtained. Then (26), as shown at the bottom of this page.

Equation (27) can be written by transforming (15). Then

$$\begin{aligned}{}^{\mathrm{B}}P_{\mathrm{F}z}^{(i)} - {}^{\mathrm{B}}P_{0z}^{(i)} &= l_{\mathrm{s}}\sin\left({\beta'}_i + \gamma_i\right) + l_{\mathrm{t}}\sin{\beta'}_i \\ &= \left(l_{\mathrm{s}}\cos\gamma_i + l_{\mathrm{t}}\right)\sin{\beta'}_i + l_{\mathrm{s}}\cos{\beta'}_i\sin\gamma_i\end{aligned} \tag{27}$$

Based on (26), the mathematical expressions can be gained. Then (28) and (29), as shown at the bottom of this page.

The mathematical expression is assumed as follows. Then

$$\xi = \left(\sqrt{\left({}^{\mathrm{B}}P_{\mathrm{F}x}^{(i)} - {}^{\mathrm{B}}P_{0x}^{(i)}\right)^2 + \left({}^{\mathrm{B}}P_{\mathrm{F}y}^{(i)} - {}^{\mathrm{B}}P_{0y}^{(i)}\right)^2} - l_{\mathrm{c}}\right)^2 + \left({}^{\mathrm{B}}P_{\mathrm{F}z}^{(i)} - {}^{\mathrm{B}}P_{0z}^{(i)}\right)^2 - l_{\mathrm{s}}^2 \tag{30}$$

Equations (28), (29), and (30) are brought into (27). Then

$$2l_{\mathrm{t}}\left({}^{\mathrm{B}}P_{\mathrm{F}z}^{(i)} - {}^{\mathrm{B}}P_{0z}^{(i)}\right) = \sqrt{4l_{\mathrm{s}}^2l_{\mathrm{t}}^2 - \left(\xi - l_{\mathrm{t}}^2\right)}\cos{\beta'}_i + \left(\xi + l_{\mathrm{t}}^2\right)\sin{\beta'}_i \tag{31}$$

$$\gamma_i = \arccos\left(\frac{\left(\sqrt{\left({}^{\mathrm{B}}P_{\mathrm{F}x}^{(i)} - {}^{\mathrm{B}}P_{0x}^{(i)}\right)^2 + \left({}^{\mathrm{B}}P_{\mathrm{F}y}^{(i)} - {}^{\mathrm{B}}P_{0y}^{(i)}\right)^2} - l_{\mathrm{c}}\right)^2 + \left({}^{\mathrm{B}}P_{\mathrm{F}z}^{(i)} - {}^{\mathrm{B}}P_{0z}^{(i)}\right)^2 - l_{\mathrm{s}}^2 - l_{\mathrm{t}}^2}{2l_{\mathrm{s}}l_{\mathrm{t}}}\right) \tag{26}$$

$$\begin{aligned}\sin\gamma_i &= \sqrt{1 - \cos^2\left(\gamma_i\right)} \\ &= \frac{\sqrt{4l_{\mathrm{s}}^2l_{\mathrm{t}}^2 - \left(\left(\sqrt{\left({}^{\mathrm{B}}P_{\mathrm{F}x}^{(i)} - {}^{\mathrm{B}}P_{0x}^{(i)}\right)^2 + \left({}^{\mathrm{B}}P_{\mathrm{F}y}^{(i)} - {}^{\mathrm{B}}P_{0y}^{(i)}\right)^2} - l_{\mathrm{c}}\right)^2 + \left({}^{\mathrm{B}}P_{\mathrm{F}z}^{(i)} - {}^{\mathrm{B}}P_{0z}^{(i)}\right)^2 - l_{\mathrm{s}}^2 - l_{\mathrm{t}}^2\right)^2}}{2l_{\mathrm{s}}l_{\mathrm{t}}}\end{aligned} \tag{28}$$

$$l_{\mathrm{s}}\cos\gamma_i + l_{\mathrm{t}} = \frac{\left(\sqrt{\left({}^{\mathrm{B}}P_{\mathrm{F}x}^{(i)} - {}^{\mathrm{B}}P_{0x}^{(i)}\right)^2 + \left({}^{\mathrm{B}}P_{\mathrm{F}y}^{(i)} - {}^{\mathrm{B}}P_{0y}^{(i)}\right)^2} - l_{\mathrm{c}}\right)^2}{2l_{\mathrm{t}}} + \frac{\left({}^{\mathrm{B}}P_{\mathrm{F}z}^{(i)} - {}^{\mathrm{B}}P_{0z}^{(i)}\right)^2 - l_{\mathrm{s}}^2 + l_{\mathrm{t}}^2}{2l_{\mathrm{t}}} \tag{29}$$

Equation (31) is transformed. The mathematical expressions can be obtained. Then

$$\begin{cases} 2l_{\mathrm{t}}\left({}^{\mathrm{B}}P_{\mathrm{F}z}^{(i)}-{}^{\mathrm{B}}P_{0z}^{(i)}\right)=\sqrt{\left(\xi+l_{\mathrm{t}}^2\right)^2+4l_{\mathrm{s}}^2l_{\mathrm{t}}^2-\left(\xi-l_{\mathrm{t}}^2\right)} \\ \qquad\qquad \times\sin\left(\beta'_i+\psi\right) \\ \psi=\arctan\frac{\sqrt{4l_{\mathrm{s}}^2l_{\mathrm{t}}^2-\left(\xi-l_{\mathrm{t}}^2\right)}}{\xi+l_{\mathrm{t}}^2} \end{cases} \tag{32}$$

According to (32), the rotation angle β'_i of hip joint can be gained. Then

$$\beta'_i=\arcsin\left(\frac{2l_{\mathrm{t}}\left({}^{\mathrm{B}}P_{\mathrm{F}z}^{(i)}-{}^{\mathrm{B}}P_{0z}^{(i)}\right)}{\sqrt{\left(\xi+l_{\mathrm{t}}^2\right)^2+4l_{\mathrm{s}}^2l_{\mathrm{t}}^2-\left(\xi-l_{\mathrm{t}}^2\right)}}\right)-\arctan\frac{\sqrt{4l_{\mathrm{s}}^2l_{\mathrm{t}}^2-\left(\xi-l_{\mathrm{t}}^2\right)}}{\xi+l_{\mathrm{t}}^2} \tag{33}$$

IV. ARTICULATED ROTATING SPEED ANALYSIS OF ROBOT WALKING SPEED CHARACTERISTICS

Based on the configuration characteristics of the large-load-ratio six-legged robot, we can conclude that the abductor joint has larger articulated displacement than the hip joint and knee joint. The weight of the robot and materials is mainly undertaken by the hip joints and knee joints. Then, we can conclude that the index of the maximum walking speed $v_{\max}$ of robot can be easily realized by the abductor joints. The technical index requiring greater torque output from joints can be achieved by rotating the hip joint and knee joint. Hence, it is helpful to avoid the same joint not only need to output a larger rotating speed but also need to output a larger articulated torque, so as to achieve the purpose of increasing the load ratio of robot.

The characteristics of the large-load-ratio six-legged robot determine that the values should be as accurate as possible in calculating the output speeds of the joints. The reason is that the larger safety margin of articulated output speed leads to the larger volume and mass for the drive devices and actuating devices. It is not conducive to improving the load ratio of robot and reducing the power consumption of mobile system. Based on the technical indexes of the large-load-ratio six-legged robot, to analyze the articulated rotating speed of single leg is actually to study the relationships between the angular velocities of rotation angles θ_i, γ_i, and β'_i and walking speed of robot. There is a linear relationship between the foot speed and the articulated rotating speed under the coordinate system $\sum_{0_i}$ for single leg. That linear relationship is called the velocity Jacobian matrix. According to (13), (14), and (15), we can conclude that the motion equations of leg i involve the generalized variable $\boldsymbol{q}$. Equation (34) can be obtained by deriving the generalized variable $\boldsymbol{q}$. Then

$$\frac{d^0\boldsymbol{P}_{\mathrm{F}}^{(i)}}{dt}=\boldsymbol{J}_i(\boldsymbol{q})\,\dot{\boldsymbol{q}} \tag{34}$$

where $d^0\boldsymbol{P}_{\mathrm{F}}^{(i)}/dt$ is the velocity matrix of foot end for the leg i. $\boldsymbol{J}_i(\boldsymbol{q})$ is the velocity Jacobian matrix of leg i. $\dot{\boldsymbol{q}}$ is the articulated velocity matrix of leg i.

The velocity Jacobian matrix of leg i is a 3×3 order matrix, and it can be written as follows. Then

$$\boldsymbol{J}_i(\boldsymbol{q})=\begin{pmatrix}\dfrac{\partial{}^{\mathrm{B}}\boldsymbol{P}_{\mathrm{F}}^{(i)}}{\partial\theta_i} & \dfrac{\partial{}^{\mathrm{B}}\boldsymbol{P}_{\mathrm{F}}^{(i)}}{\partial\beta'_i} & \dfrac{\partial{}^{\mathrm{B}}\boldsymbol{P}_{\mathrm{F}}^{(i)}}{\partial\gamma_i}\end{pmatrix}\in\boldsymbol{R}^{3\times3} \tag{35}$$

where

$$\frac{\partial{}^{\mathrm{B}}P_{\mathrm{F}}^{(i)}}{\partial\theta_i}=\begin{pmatrix}-l_{\mathrm{s}}\sin\left(\Phi_i+\theta_i\right)\cos\beta_i-\left(l_{\mathrm{t}}\cos\beta'_i+l_{\mathrm{c}}\right)\sin\left(\Phi_i+\theta_i\right)\\ l_{\mathrm{s}}\cos\left(\Phi_i+\theta_i\right)\cos\beta_i+\left(l_{\mathrm{t}}\cos\beta'_i+l_{\mathrm{c}}\right)\cos\left(\Phi_i+\theta_i\right)\\ 0\end{pmatrix}$$

$$\frac{\partial{}^{\mathrm{B}}P_{\mathrm{F}}^{(i)}}{\partial\beta'_i}=\begin{pmatrix}-l_{\mathrm{s}}\cos\left(\Phi_i+\theta_i\right)\sin\left(\beta'_i+\gamma_i\right)-l_{\mathrm{t}}\cos\left(\Phi_i+\theta_i\right)\sin\beta'_i\\ -l_{\mathrm{s}}\sin\left(\Phi_i+\theta_i\right)\sin\left(\beta'_i+\gamma_i\right)-l_{\mathrm{t}}\sin\left(\Phi_i+\theta_i\right)\sin\beta'_i\\ l_{\mathrm{s}}\cos\left(\beta'_i+\gamma_i\right)+l_{\mathrm{t}}\cos\beta'_i\end{pmatrix}$$

$$\frac{\partial{}^{\mathrm{B}}P_{\mathrm{F}}^{(i)}}{\partial\gamma_i}=\begin{pmatrix}-l_{\mathrm{s}}\cos\left(\Phi_i+\theta_i\right)\sin\left(\beta'_i+\gamma_i\right)\\ -l_{\mathrm{s}}\sin\left(\Phi_i+\theta_i\right)\sin\left(\beta'_i+\gamma_i\right)\\ l_{\mathrm{s}}\cos\left(\beta'_i+\gamma_i\right)\end{pmatrix}$$

When the velocity matrix of foot end of the leg i is obtained for the large-load-ratio six-legged robot, the articulated speed matrix can be written for actualizing the accurate control of leg i based on (34) and (35). Then

$$\dot{\boldsymbol{q}}=\boldsymbol{J}_i(\boldsymbol{q})^{-1}\frac{d^0\boldsymbol{P}_{\mathrm{F}}^{(i)}}{dt} \tag{36}$$

A. ROTATING SPEED ANALYSIS OF ABDUCTOR JOINT

1) ROTATING SPEED ANALYSIS OF ABDUCTOR JOINT UNDER D-H METHOD

Since the homogeneous joints of the large-load-ratio six-legged robot have the same drive devices and actuating devices, the articulated rotating speed analysis of leg 5 is carried out to provide data support for the joint selection and design of robot. Based on Figure 5, it is assumed that the robot walks in a straight line at a constant speed of v_{R} along the Y_{B} axis of the body coordinate system. The trajectories formed by the footing points of six legs on the ground are parallel to the Y_{B} axis. Due to the contact between the legs in the support phase and the ground, we can conclude that the linear velocities v_x in the directions of X_{B} and v_z in the directions of Z_{B} are both zero for the foot end of leg 5. The value of linear velocity v_y in the direction of Y_{B} is the same as that of the robot, but the direction is opposite.

Based on (1), (34), (35), and the above analysis, the velocity matrix of foot end of the leg 5 can be written as follows.

Then

$$\begin{pmatrix} v_{5x} \\ v_{5y} \\ v_{5z} \end{pmatrix} = \begin{pmatrix} R_{11} & R_{12} & R_{13} \\ R_{21} & R_{22} & R_{23} \\ 0 & R_{32} & R_{33} \end{pmatrix} \begin{pmatrix} \dot{\theta}_5 \\ \dot{\beta}'_5 \\ \dot{\gamma}_5 \end{pmatrix} \tag{37}$$

where

$$\begin{aligned} R_{11} &= -l_s \sin\theta_5 \cos\beta_5 - \sin\theta_5 \left(l_t \cos\beta'_5 + l_c\right) \\ R_{12} &= -l_s \cos\theta_5 \sin\beta_5 - l_t \cos\theta_5 \sin\beta'_5 \\ R_{13} &= -l_s \cos\theta_5 \sin\beta_5 \\ R_{21} &= l_s \cos\theta_5 \cos\beta_5 + \cos\theta_5 \left(l_t \cos\beta'_5 + l_c\right) \\ R_{22} &= -l_s \sin\theta_5 \sin\beta_5 - l_t \sin\theta_5 \sin\beta'_5 \\ R_{23} &= -l_s \sin\theta_5 \sin\beta_5 \\ R_{32} &= l_s \cos\beta_5 + l_t \cos\beta'_5 \\ R_{33} &= l_s \cos\beta_5 \end{aligned}$$

When the walking speed v_R is equal to the maximum walking speed v_{max} of robot, the mathematical expressions can be obtained based on (37). Then

$$\begin{cases} v_{5x} = \sin\theta_5 \left(l_s \cos\beta_5 + l_t \cos\beta'_5 + l_c\right) \dot{\theta}_5 + \cos\theta_5 \\ \quad \times \left(l_s \sin\beta_5 + l_t \sin\beta'_5\right) \dot{\beta}'_5 + \cos\theta_5 \left(l_s \sin\beta_5\right) \dot{\gamma}_5 = 0 \\ v_{5y} = \cos\theta_5 \left(l_s \cos\beta_5 + l_t \cos\beta'_5 + l_c\right) \dot{\theta}_5 - \sin\theta_5 \left(l_s \right. \\ \quad \left. \times \sin\beta_5 + l_t \sin\beta'_5\right) \dot{\beta}'_5 - \sin\theta_5 \left(l_s \sin\beta_5\right) \dot{\gamma}_5 = -v_{max} \\ v_{5z} = \left(l_s \cos\beta_5 + l_t \cos\beta'_5\right) \dot{\beta}'_5 + \left(l_s \cos\beta_5\right) \dot{\gamma}_5 = 0 \end{cases} \tag{38}$$

Based on (38), the rotation speeds of the abductor joint, hip joint, and knee joint can be acquired for the leg 5. Then

$$\begin{cases} \dot{\theta}_5 = -v_{max} \cos\theta_5 \big/ \left(l_s \cos\beta_5 + l_t \cos\beta'_5 + l_c\right) \\ \dot{\beta}'_5 = -v_{max} \sin\theta_5 \cos\beta_5 / \left(l_t \sin\gamma_5\right) \\ \dot{\gamma}_5 = v_{max} \sin\theta_5 \left(l_s \cos\beta_5 + l_t \cos\beta'_5\right) / \left(l_t l_s \sin\gamma_5\right) \gamma_5 \neq 0° \end{cases} \tag{39}$$

When the linear velocity of foot end is known and the steering of joint is not considered, the values of articulated rotating speeds at any time can be directly obtained through (39). Based on the structure parameters of robot, index of maximum walking speed, and ranges of articulated rotation angles, Equation (39) can be used to obtain the variable ranges of the rotating speeds R_A, R_H, R_K of the abductor joint, hip joint, and knee joint. Figures 8, 9, and 10 show the variable range charts of rotating speeds for the abductor joint, hip joint, and knee joint, respectively.

According to Figure 8, we can obtain that the maximum rotating speed of abductor joint is 7.4 r/min. The denominator parts of mathematical expressions contains $\sin\gamma_i$ term for the rotating speeds of the hip joint and knee joint. When the value of γ_i tends to zero, the hip joint, knee joint, and foot end of robot tend to be collinear. Then, the rotating speeds exist the maximum values and have more selected space for the hip joint and knee joint. Therefore, the range of the rotating speed of abductor joint can be easily obtained according to (39), but the maximum rotating speeds of the hip joint and knee joint are not easy to be determined.

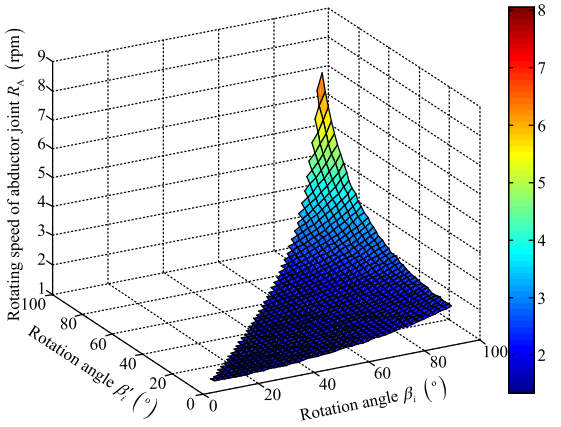

FIGURE 8. Variable range chart of rotating speed R_A of abductor joint with changes in β'_i and β_i.

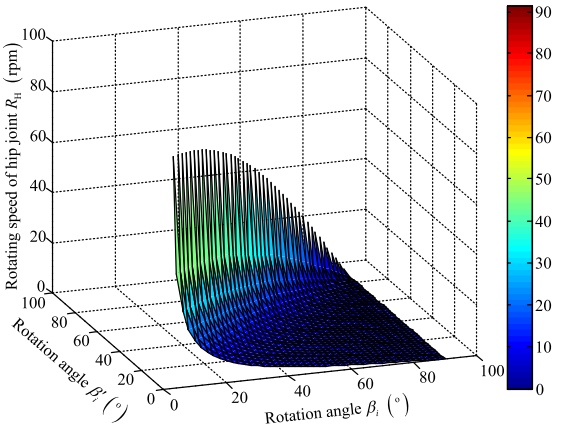

FIGURE 9. Variable range chart of rotating speed R_H of hip joint with changes in β'_i and β_i.

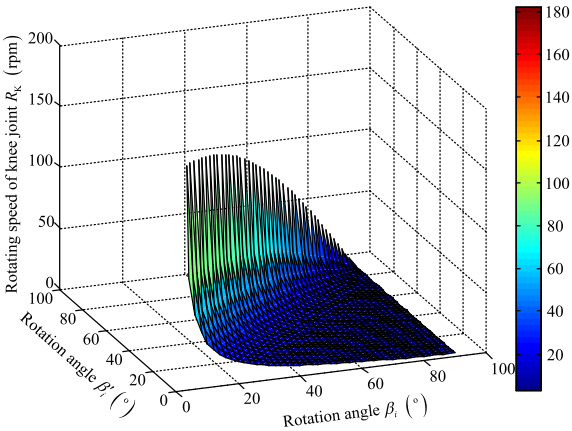

FIGURE 10. Variable range chart of rotating speed R_K of knee joint with changes in β'_i and β_i.

Based on Figures 8, 9, and 10, we can conclude that only rotating speed of abductor joint can be effectively confirmed in a single leg according to (39). The rotating speeds of hip joint and knee joint can not be ascertained. Although the D-H method is systematic, its solving process is relatively

complex in the articulated rotating speed. The reason is that the large number of formula transformations are involved in the forward kinematics and inverse kinematics analyses. It is not conducive to the development of the multi-legged robots, especially for the large-load-ratio multi-legged robots.

Due to the unsuitability of the D-H method in calculating the rotating speeds of the hip joints and knee joints, the maximum walking speed method is proposed. Through rotating one of the joints to achieve the maximum speed index of robot, the maximum walking speed method is employed to establish the mathematical relationships between the articulated rotating angles and the maximum walking speed index of robot. The maximum walking speed method can quickly obtain the required output rotating speed of each joint.

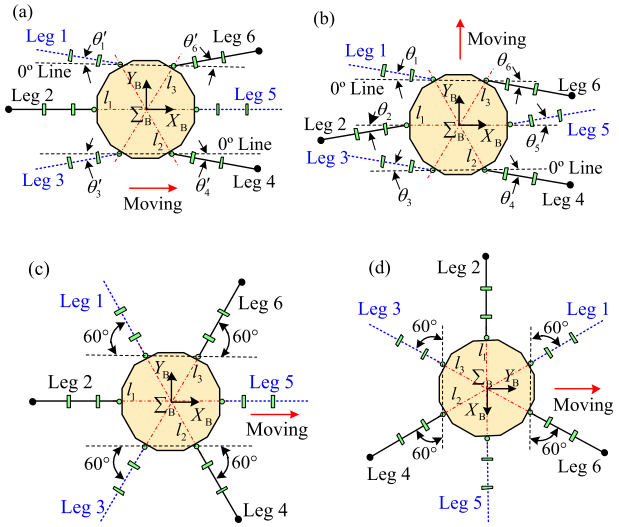

FIGURE 11. Four kinds of walking modes under the tripod gait: (a) crab type, (b) ant type, (c) crab–ant mixed type I, and (d) crab–ant mixed type II.

2) ROTATING SPEED ANALYSIS OF ABDUCTOR JOINT UNDER MAXIMUM WALKING SPEED METHOD

The tripod gait is the common and fastest gait of the six-legged robots and hexapod insects [28]–[30] Namely, the efficiency of robot walking is higher when the duty ratio β_R is 0.5. Compared with the quadrangular gait and pentagon gait, it is easier to achieve the maximum walking speed v_{max} of large-load-ratio six-legged robot according to the tripod gait. Based on the configuration characteristics of large-load-ratio six-legged robot, the walking modes under the tripod gait can be divided into the crab type, ant type, crab–ant mixed type I, and crab–ant mixed type II; they are shown in Figure 11. When the large-load-ratio six-legged robot walks under the ant-type tripod gait, the maximum walking speed v_{max} of robot is mainly realized by rotating the abductor joints. The hip joints and knee joints do not take the main role in the walking speed of robot. In Figure 11, the straight lines l_1, l_2, and l_3 are orthogonal to the relevant axes of the abductor joints.

To conveniently carry out the analysis, the legs 2, 4 and 6 in the support phase at a certain time are regarded as the first group. The legs 1, 3 and 5 in the transfer phase are viewed as the second group. To reduce the analysis redundancy, it is assumed that the homogeneous joints in the same phase have the equal rotating angles. The initial angles θ_i of abductor joints are assumed as 0° for the legs 1–6. The rotation angles θ_i' and θ_i of the abductor joint are between the leg i and 0° line under the crab-type and ant-type tripod gait, respectively. Due to the same homogeneous joints in six legs, the rotating speed analysis of abductor joint is carried out based on the leg 5. Figure 12 illustrates the scheme of rotation angle analysis for the abductor joint.

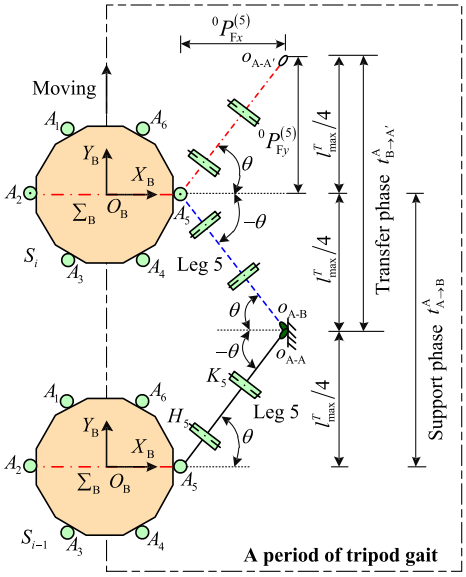

FIGURE 12. Scheme of rotation angle analysis for abductor joint.

Based on Figure 12, a period of tripod gait can be obtained from the state S_{i-1} to state S_i for the leg 5. The rotation angle of abductor joint has two extreme positions: front swing angle $+\theta$ and rear swing angle $-\theta$. The values of rotation angles are the same between $+\theta$ and $-\theta$. The support foot moves from point o_{A-A} to point o_{A-B} (actually, two support point are coincidence), and then from point o_{A-B} to point $o_{A-A'}$, which is called one step. $t^{A}_{A\to B}$ and $t^{A}_{B\to A'}$ are respectively regarded as the load time and no-load time when the support foot moves from point o_{A-A} to point o_{A-B} and from point o_{A-B} to point $o_{A-A'}$. The maximum walking distance l^{T}_{max} of robot is $v_{max}T$ in a period T of gait. Hence, the walking distance of robot is $v_{max}T/2$ by rotating the abductor joint of leg 5 in time $t^{A}_{A\to B}$.

According to Figure 7 and (20), the mathematical expression of rotation angle can be written for the abductor joint of leg 5. Then

$$\theta_5 = \arctan\left(\frac{{}^{B}P^{(5)}_{Fy} - {}^{B}P^{(5)}_{0y}}{{}^{B}P^{(5)}_{Fx} - {}^{B}P^{(5)}_{0x}}\right) - \Phi_5 = \arctan\left(\frac{{}^{0}P^{(5)}_{Fy}}{{}^{0}P^{(5)}_{Fx}}\right) \quad (40)$$

The abductor joints of six legs have the same drive devices and actuating devices. According to Figure 12 and (40),

the solution of the rotation angle of abductor joint can be transformed as follows. Then

$$\theta_5 = \arcsin\left(\frac{{}^0P_{\mathrm{Fy}}^{(5)}}{\left(l_{\mathrm{c}} + l_{\mathrm{t}}\cos\beta'_i + l_{\mathrm{s}}\cos\beta_i\right)}\right) = \arcsin\left(\frac{v_{\max}T}{4\left(l_{\mathrm{c}} + l_{\mathrm{t}}\cos\beta'_i + l_{\mathrm{s}}\cos\beta_i\right)}\right) = \theta_i \quad (41)$$

According to (41), we can conclude that the abductor joint rotates the angle of θ in time $T/4$. Therefore, the rotational number of abductor joint can be determined in the 1 min. The gait period T is assumed 1 s. Based on (41), technical parameters of robot, and constraint condition: $0° \le \beta'_i \le \beta_i \le 90°$, Matlab software is employed to analyze the variable ranges of the rotation angle θ and rotating speed R_{A} of abductor joint with the changes in the rotation angle β'_i of hip joint and rotation angle β_i of knee joint. Figures 13 and 14 show the variable range charts of the rotation angle θ and rotating speed R_{A}.

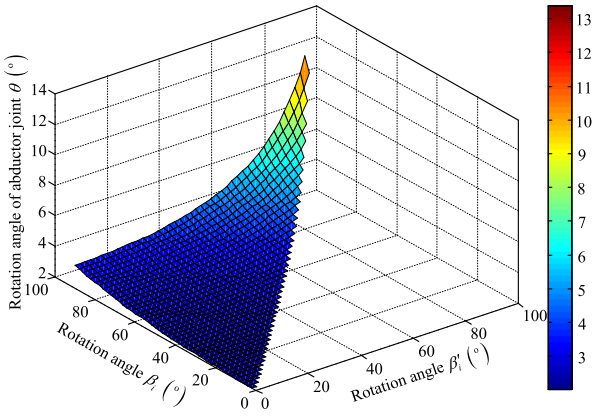

FIGURE 13. Variable range chart of rotation angle of abductor joint with changes in β'_i and β_i.

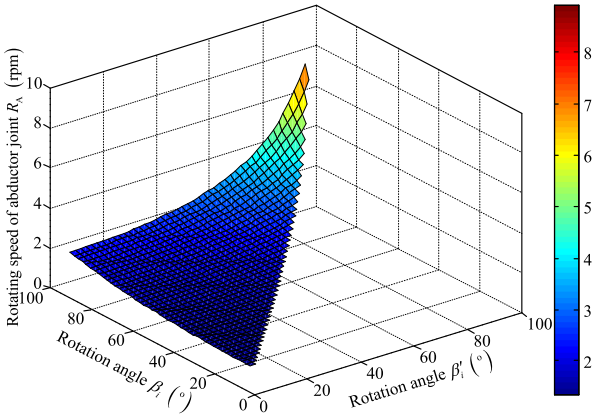

FIGURE 14. Variable range chart of rotating speed of abductor joint with changes in β'_i and β_i.

According to Figures 13 and 14, the variable tendencies of the rotation angle θ and rotating speed R_{A} move gradually augmentation with the increases of β'_i and β_i. The maximum rotating speed of abductor joint is 8.1 r/min, which is larger than the maximum rotating speed 7.4 r/min of abductor joint in Figure 8. The analysis error is 9%. Then, the validity of the proposed analysis method of articulated rotating speed is verified and can be applied to the rotating speed analyses of the hip joint and knee joint. To ensure that the robot can achieve the maximum walking speed $v_{\max}$ and reduce the influences of external factors, such as feedback error of control system, external disturbance, etc., the safety factor is determined to be 1.3 in the design of the drive devices and actuating devices of joints.

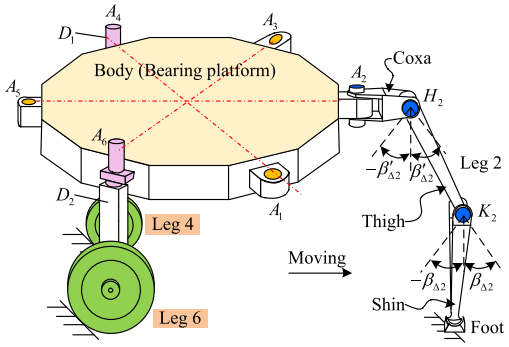

FIGURE 15. Equivalent scheme of support phase under carb-type tripod gait.

B. ROTATING SPEED ANALYSIS OF HIP JOINT

In view of the geometric analysis method of the rotating speed of abductor joint, the ranges of the rotating speeds for the hip joint and knee joint are respectively calculated by using the crab-type tripod gait. When the large-load-ratio six-legged robot walks under the crab-type tripod gait, the support phase of robot can be equivalent to two wheels and one leg. Figure 15 illustrates the equivalent scheme of the support phase under carb-type tripod gait. The rotation angles of abductor joints are set to 0° for the legs 1–6. The devices D_1 and D_2 are installed at the abductor joints A_4 and A_6. The two wheels can only move forward or backward. The Connecting line of wheel cores is perpendicular to the forward direction of robot. The devices D_1 and D_2 can automatically adjust the heights of wheels to adapt the height change of body when the robot moves forward or backward. The abductor joint of leg 2 is locked. The drive devices and actuating devices only work for the hip joint and knee joint of leg 2. Other influence factors are not considered or considered as having no effect on the equivalent system. When the hip joint and knee joints are rotated separately to achieve the maximum walking speed $v_{\max}$ of robot, the required rotation speed of the hip joint and knee joint can be obtained.

Based on Figure 15, the knee joint is locked. The hip joint is only rotated to achieve the maximum walking speed $v_{\max}$ of the large-load-ratio six-legged robot. When the thigh and shin are collinear, there is the longest effective distance from the rotating axis of the hip joint to the foot end. Then, the minimum and maximum rotating speeds can be respectively obtained for the hip joint.

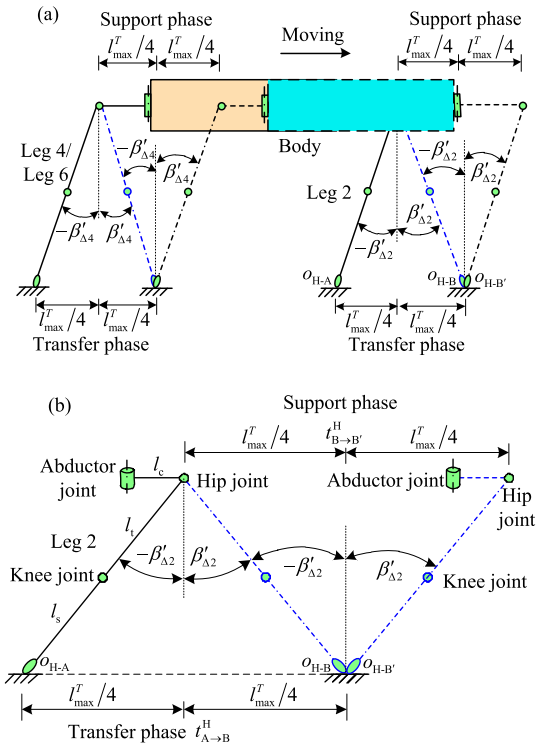

FIGURE 16. Scheme of minimum rotating speed analysis for hip joint: (a) walking of robot by rotating hip joints and (b) contribution of hip joint of leg 2 for walking of robot.

1) MINIMUM ROTATING SPEED ANALYSIS OF HIP JOINT

Figure 16 illustrates the scheme of the minimum rotating speed analysis of hip joint. In Figure 16, the rotation angle of hip joint of the leg i contains the front rotation angle $\beta'_{\Delta i}$ and rear rotation angle $-\beta'_{\Delta i}$. The range of $\beta'_{\Delta i}$ is from 0° to 45°. Due to the equal rotation angles of joints for the homogeneous joints in the same phase, we can conclude that the relational expressions are $\beta'_{\Delta 2} = \beta'_{\Delta 4} = \beta'_{\Delta 6}$ and $-\beta'_{\Delta 2} = -\beta'_{\Delta 4} = -\beta'_{\Delta 6}$.

In Figure 16, the solid line represents the front half posture of robot in a gait period. The dashed line represents the rear half posture of robot in a gait period. We can know that a step of robot contains from point $o_{\mathrm{H-A}}$ to point $o_{\mathrm{H-B}}$ and from point $o_{\mathrm{H-B}}$ to point $o_{\mathrm{H-B'}}$ for the support foot of leg 2. Actually, the point $o_{\mathrm{H-B}}$ coincides with point $o_{\mathrm{H-B'}}$. Then, The maximum walking distance $l^T_{\max}$ of robot is $v_{\max}T$ in a gait period T. $t^{\mathrm{H}}_{\mathrm{A}\to\mathrm{B}}$ and $t^{\mathrm{H}}_{\mathrm{B}\to\mathrm{B'}}$ are respectively viewed as the no-load time and load time when the support foot of leg 2 moves from point $o_{\mathrm{H-A}}$ to point o_{HB} and from point $o_{\mathrm{H-B}}$ to point $o_{\mathrm{H-B'}}$. We can see that the walking distance of robot is $v_{\max}T/2$ in time $t^{\mathrm{H}}_{\mathrm{B}\to\mathrm{B'}}$

Based on Figure 16, The geometric relations can be obtained as follows. Then

$$\sin\beta'_{\Delta 2} = \frac{v_{\max}T}{4l_{\mathrm{t}} + 4l_{\mathrm{c}}} = 0.0417 \tag{42}$$

The value of gait period T is set to 1 s. Then, we can obtain that the value of $\beta'_{\Delta 2}$ is 2.3885°. The rotating speed of hip joint is 1.5923 r/min.

According to Figure 16, the mathematical relationship between the walking speed v of robot and the rotating speed n_{r} of hip joint can be expressed as follows. Then

$$n_r/60 = v/2\pi r \tag{43}$$

where n_{r} is the rotating speed of hip joint, r/min. v is the walking speed of robot, m/s. r is the vertical distance from the axis of hip joint to the line $\overline{o_{\mathrm{H-A}}o_{\mathrm{H-B}}}$, m.

Based on (42) and (43), the walking speed v of robot can be gained as follows. Then

$$v = \frac{2\pi\,(l_{\mathrm{t}} + l_{\mathrm{s}})\,n_{\mathrm{r}}\cos\beta'_{\Delta 2}}{60} \approx v_{\max} \tag{44}$$

According to (44), we can conclude that the robot can achieve the maximum walking speed $v_{\max}$ at the minimum rotating speed of 1.5923 r/min with only rotating the hip joint.

2) MAXIMUM ROTATING SPEED ANALYSIS OF HIP JOINT

When the range of $\beta'_{\Delta i}$ is from 45° to 90°, the maximum walking speed $v_{\max}$ of robot can be actualized by rotating the hip joint. The hip joint has the maximum rotating speed because the rotating arc length of foot end is greater in the vertical direction than in the horizontal direction. Figure 17 illustrates the scheme of maximum rotating speed analysis for the hip joint.

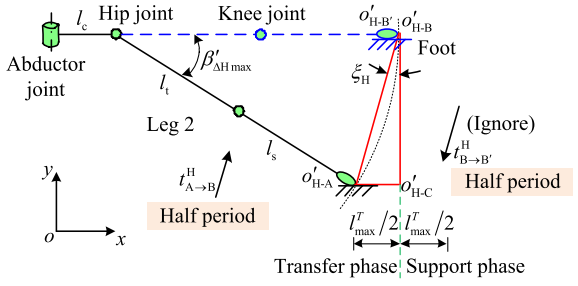

FIGURE 17. Scheme of maximum rotating speed analysis for hip joint.

The solution method of the maximum rotating speed of hip joint is basically the same as that of the minimum rotating speed. It is assumed that the leg 2 of robot can swing to the maximum level. The maximum walking distance $l^T_{\max}$ of robot is $v_{\max}T$ in a gait period T. The walking distance of robot is $v_{\max}T/2$ when the value of rotation angle of the hip joint is $\beta'_{\Delta Hmax}$ in the support phase. Based on Figure 17, the projection of connection line between point $o'_{\mathrm{H-A}}$ and point $o'_{\mathrm{H-B}}$ is $o'_{\mathrm{H-A}}o'_{\mathrm{H-C}}$ in the x direction, and its length is $v_{\max}T/2$. The value of included angle $\angle o'_{\mathrm{H-A}}o'_{\mathrm{H-B}}o'_{\mathrm{H-C}}$ is set to ξ_{H}. The projection is $o'_{\mathrm{H-B}}o'_{\mathrm{H-C}}$ in the y direction. The rotation angle $\beta'_{\Delta Hmax}$ is assumed as very small. Hence, we can obtain that the geometric relations are $=\overline{o'_{\mathrm{H-A}}o'_{\mathrm{H-B}}}$ and $\beta'_{\Delta Hmax} = 2\xi_{\mathrm{H}}$. Due to the small angle ξ_{H}, it can be

approximated as $\overline{o'_{\mathrm{H-B}}o'_{\mathrm{H-C}}} = \overline{o'_{\mathrm{H-A}}o'_{\mathrm{H-B}}}$. Meanwhile, the constraint conditions are $0° \le \xi_{\mathrm{H}} \le 45°$ and $0° \le \beta'_{\Delta Hmax} \le 90°$. According to Figure 17, the mathematical expressions can be written as follows. Then

$$\begin{cases} \beta'_{\Delta\mathrm{Hmax}} = 2\xi_{\mathrm{H}} \\ \sin\frac{\xi_{\mathrm{H}}}{2} = \frac{v_{\max}T}{\frac{4\pi(l_{\mathrm{t}}+l_{\mathrm{c}})\beta'_{\Delta\mathrm{Hmax}}}{180}} \end{cases} \tag{45}$$

The value of gait period T is set to 1 s. Then, we can obtain that the value of $\beta'_{\Delta Hmax}$ is 23.42°. The rotating speed of hip joint is 7.8067 r/min. The maximum walking speed $v_{\max}$ of robot can be realized by only rotating hip joint. Based on (45), the walking speed v of robot can be gained as follows. Then

$$\begin{aligned} v &= \frac{2\pi n_{\mathrm{r}}\overline{o'_{\mathrm{H-A}}o'_{\mathrm{H-B}}}\cos\xi_{\mathrm{H}}}{60} \\ &= \frac{2\pi^2 n_{\mathrm{r}}(l_{\mathrm{t}}+l_{\mathrm{c}})\beta'_{\Delta\mathrm{Hmax}}\cos\xi_{\mathrm{H}}}{60\times 180} \approx 1.96 v_{\max} \end{aligned} \tag{46}$$

According to (46), we can conclude that the maximum walking speed of robot is 1.96 times that of $v_{\max}$. The reasons for the error are due to the approximate equivalence in the analysis process. On the one hand, the rotation angle of 23.42° for hip joint is very big. So there is error in equivalence for $\overline{o'_{\mathrm{H-A}}o'_{\mathrm{H-B}}}$, which leads to the larger distance between point $o'_{\mathrm{H-A}}$ and point $o'_{\mathrm{H-B}}$ than the actual distance between two points. On the other hand, there is error in $\overline{o'_{\mathrm{H-B}}o'_{\mathrm{H-C}}}$ equivalence for $\overline{o'_{\mathrm{H-A}}o'_{\mathrm{H-B}}}$, which results in the larger distance between point $o'_{\mathrm{H-A}}$ and point $o'_{\mathrm{H-C}}$ than the actual distance between two points. When the rotating speed of hip joint is divided by multiple $\sqrt{2}$ based on the above calculation results, we can obtain that the rotating speed of hip joint is 5.5210 r/min. The values of $\beta'_{\Delta Hmax}$ and ξ_{H} are 16.5630° and 8.2815°. Based on (46), we can conclude that the maximum walking speed of robot is approximately equal to $v_{\max}$.

To summarize, the range of rotating speed of the hip joint is from 1.5923 r/min to 5.5210 r/min, when the robot walks under the carb-type tripod gait and the hip joints are only rotated to achieve the maximum walking speed $v_{\max}$ of robot. The safety factor does not need to be selected in the design of the rotating speed of hip joint. The reason is that the maximum walking speed of robot is not the main responsibility of the hip joint.

C. ROTATING SPEED ANALYSIS OF KNEE JOINT

Based on Figure 15 and the rotating speed analysis method of hip joint, the rotating speed analysis of knee joint is carried out. The knee joint has the minimum and maximum rotating speeds when the knee joint is only employed to realize the maximum walking speed $v_{\max}$ of robot.

1) MINIMUM ROTATING SPEED ANALYSIS OF KNEE JOINT

The walking speed of robot is fully provided by the knee joint when the hip joint is locked. The rotation angle of knee joint of the leg i includes the front rotation angle $\beta_{\Delta i}$ and rear rotation angle $-\beta_{\Delta i}$. The constraint condition is $0° \le \beta_{\Delta i} \le 45°$. Due to the equal rotation angles of joints for the homogeneous joints in the same phase, we can conclude that the relational expressions are $\beta_{\Delta 2} = \beta_{\Delta 4} = \beta_{\Delta 6}$ and $-\beta_{\Delta 2} = -\beta_{\Delta 4} = -\beta_{\Delta 6}$. Figure 18 illustrates the scheme of the minimum rotating speed analysis of knee joint.

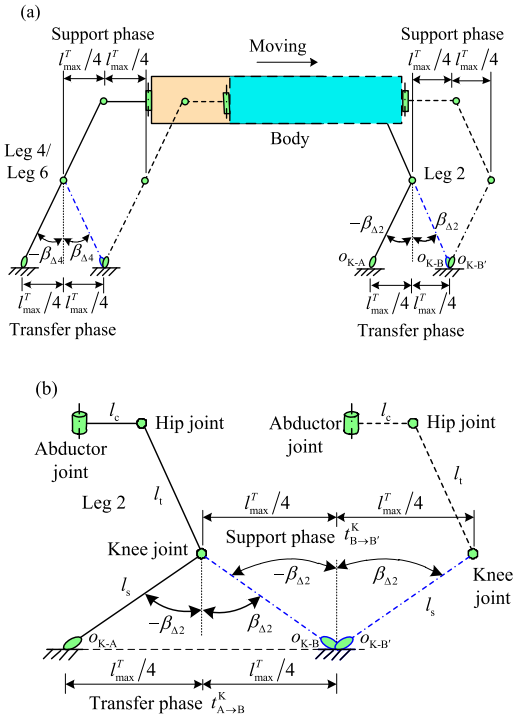

FIGURE 18. Scheme of minimum rotating speed analysis for knee joint: (a) walking of robot by rotating knee joints and (b) contribution of knee joint of leg 2 for walking of robot.

In Figure 18, the solid line represents the front half posture of robot in a gait period. The dashed line represents the rear half posture of robot in a gait period. We can know that a step of robot contains from point $o_{\mathrm{K-A}}$ to point $o_{\mathrm{K-B}}$ and from point $o_{\mathrm{K-B}}$ to point $o_{\mathrm{K-B'}}$ for the support foot of leg 2. Actually, the point $o_{\mathrm{K-B}}$ coincides with point $o_{\mathrm{K-B'}}$. Then, The maximum walking distance $l^T_{\max}$ of robot is $v_{\max}T$ in a gait period T. $t^{\mathrm{K}}_{\mathrm{A\to B}}$ and $t^{\mathrm{K}}_{\mathrm{B\to B'}}$ are respectively viewed as the no-load time and load time when the support foot of leg 2 moves from point $o_{\mathrm{K-A}}$ to point o_{KB} and from point $o_{\mathrm{K-B}}$ to point $o_{\mathrm{K-B'}}$. We can see that the walking distance of robot is $v_{\max}T/2$ in time $t^{\mathrm{K}}_{\mathrm{B\to B'}}$. Based on Figure 18, the geometric relations can be obtained as follows. Then

$$\sin\beta_{\Delta 2} = \frac{v_{\max}T}{4l_{\mathrm{s}}} = 0.0833 \tag{47}$$

The value of gait period T is set to 1 s. Then, we can obtain that the value of $\beta_{\Delta 2}$ is 4.7812°. The rotating speed of knee joint is 3.1875 r/min. Based on (47), the walking speed v of robot can be gained as follows. Then

$$v = \frac{2\pi l_{\mathrm{s}} n_{\mathrm{r}}\cos\beta_{\Delta 2}}{60} \approx v_{\max} \tag{48}$$

According to (48), we can conclude that the robot can achieve the maximum walking speed $v_{\max}$ at the minimum rotating speed of 3.1875 r/min with only rotating the knee joint.

2) MAXIMUM ROTATING SPEED ANALYSIS OF KNEE JOINT

When the range of $\beta_{\Delta i}$ is from 45° to 90°, the maximum walking speed $v_{\max}$ of robot can be actualized by rotating the knee joint. The knee joint has the maximum rotating speed because the rotating arc length of foot end is greater in the vertical direction than in the horizontal direction. Figure 19 illustrates the scheme of maximum rotating speed analysis for the knee joint.

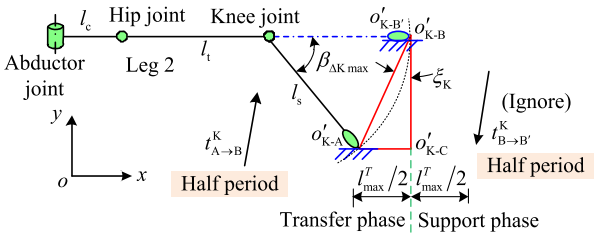

FIGURE 19. Scheme of maximum rotating speed analysis for knee joint.

The solution method of the maximum rotating speed of knee joint is basically the same as that of the minimum rotating speed. It is assumed that the leg 2 of robot can swing to the maximum level. The maximum walking distance $l^T_{\max}$ of robot is $v_{\max}T$ in a gait period T. The walking distance of robot is $v_{\max}T/2$ when the value of rotation angle of the knee joint is $\beta_{\Delta Kmax}$ in the support phase. Based on Figure 19, the projection of connection line between point o'_{K-A} and point o'_{K-B} is $o'_{K-A}o'_{K-C}$ in the x direction, and its length is $v_{\max}T/2$. The value of included angle $\angle o'_{K-A}o'_{K-B}o'_{K-C}$ is set to ξ_K. The projection is $o'_{K-B}o'_{K-C}$ in the y direction. The rotation angle $\beta_{\Delta Kmax}$ is assumed as very small. Hence, we can obtain that the geometric relations are $=\overline{o'_{K\text{-}A}o'_{K\text{-}B}}$ and $\beta_{\Delta Kmax} = 2\xi_K$. Due to the small angle ξ_K, it can be approximated as $\overline{o'_{K\text{-}B}o'_{K\text{-}C}} = \overline{o'_{K\text{-}A}o'_{K\text{-}B}}$. Meanwhile, the constraint conditions are $0° \le \xi_K \le 45°$ and $0° \le \beta_{\Delta Kmax} \le 90°$. According to Figure 19, the mathematical expressions can be written as follows. Then

$$\begin{cases} \beta_{\Delta K\max} = 2\xi_K \\ \sin\dfrac{\xi_K}{2} = \dfrac{v_{\max}T}{\dfrac{4\pi l_s \beta_{\Delta K\max}}{180}} \end{cases} \tag{49}$$

The value of gait period T is set to 1 s. Then, we can obtain that the value of $\beta_{\Delta Kmax}$ is 33.1407°. The rotating speed of knee joint is 11.0469 r/min. The maximum walking speed $v_{\max}$ of robot can be realized by only rotating knee joint. Based on (49), the walking speed v of robot can be gained as follows. Then

$$\begin{aligned} v &= \frac{2\pi n_r \overline{o'_{K\text{-}A}o'_{K\text{-}B}}\cos\xi_K}{60} \\ &= \frac{2\pi^2 l_s n_r \beta_{\Delta K\max}\cos\xi_K}{60\times 180} \approx 1.92 v_{\max} \end{aligned} \tag{50}$$

According to (50), we can conclude that the maximum walking speed of robot is 1.96 times that of $v_{\max}$. The reasons for the error are due to the approximate equivalence in the analysis process. On the one hand, the rotation angle of 33.1407° for knee joint is very big. So there is error in equivalence for $\overline{o'_{K\text{-}A}o'_{K\text{-}B}}$, which leads to the larger distance between point o'_{K-A} and point o'_{K-B} than the actual distance between two points. On the other hand, there is error in $\overline{o'_{K\text{-}B}o'_{K\text{-}C}}$ equivalence for $\overline{o'_{K\text{-}A}o'_{K\text{-}B}}$, which results in the larger distance between point o'_{K-A} and point o'_{K-C} than the actual distance between two points. When the rotating speed of knee joint is divided by multiple $\sqrt{2}$ based on the above calculation results, we can obtain that the rotating speed of knee joint is 7.8113 r/min. The values of $\beta_{\Delta Kmax}$ and ξ_K are 23.4339° and 11.7170°. Based on (50), we can conclude that the maximum walking speed of robot is approximately equal to $v_{\max}$.

To summarize, the range of rotating speed of the knee joint is from 3.1875 r/min to 7.8113 r/min, when the robot walks under the carb-type tripod gait and the knee joints are only rotated to achieve the maximum walking speed $v_{\max}$ of robot. The safety factor does not need to be selected in the design of the rotating speed of knee joint. The reason is that the maximum walking speed of robot is not the main responsibility of the knee joint.

To sum up the above analyses of the articulated rotating speed ranges for the abductor joint, hip joint, and knee joint, we can conclude that the maximum walking speed method can quickly and accurately obtain the ranges of articulated rotating speeds by comparing with the traditional D-H method, which is propitious to provide the data support for reasonable matching the drive devices and actuating devices of joints. Although the D-H method is systematic, it is relatively complex and involves the large number of formula transformations. The maximum walking speed method only refers to simple geometric relations. Then, we can quickly obtain the ranges of the output speeds of all joints by simple geometric calculation. Meanwhile, the analysis error is 9% on the maximum rotating speed of abductor joint by comparing the D-H method with the maximum walking speed method. Hence, it can be said that the maximum walking speed method is the rapidity, accuracy, and conciseness

V. SIMULATION VERIFICATION OF ROBOT WALKING

The rotating speed analyses of the hip joint and knee joint mainly provide the data basis for matching their drive devices and actuating devices. In practice, there is no situation that only the hip joint or knee joint is used for robot walking. According to the rotating speed analysis of abductor joint, besides the matching selection of the drive device and actuating device at abductor joint, another point is to achieve the maximum walking speed index $v_{\max}$ of robot. Next, the simulation analysis of robot walking is actualized to verify the rationality of theoretical analysis for the abductor joint.

Based on Figures 13 and 14, we can obtain the pose of robot under the 1.3 $v_{\max}$; they are $\beta'_i = 45°$ and $\beta_i = 60°$.

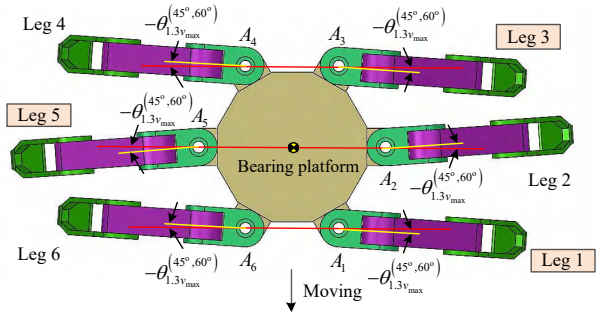

FIGURE 20. Pose of robot under a certain time state.

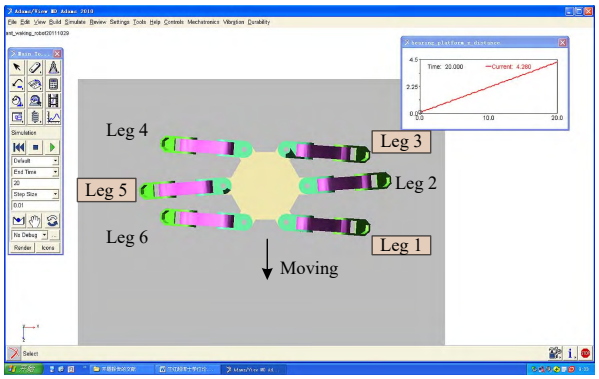

FIGURE 21. Virtual simulation of robot walking.

Then, the 3D model of virtual prototype is constructed and imported into ADAMS software. The front swing angle of abductor joint is set to $\theta_{1.3v_{\max}}^{(45^\circ,60^\circ)}$ under the $1.3v_{\max}$. The rotation trajectories are set as the cosine periodic functions for the abductor joint, hip joint, and knee joint. The hip joint and knee joint assist with the rotating of abductor joint to achieve the maximum walking speed index $v_{\max}$ of robot. Due to the reciprocating switching of single leg between the transfer phase and the support phase under the tripod gait there is a difference of half a period for the periodic functions of abductor joints among the adjacent legs To facilitate the simulation verification of robot walking, the pose of robot is set to a certain time state; it is shown in Figure 20. In Figure 16, the legs 1, 3, and 5 just enter the support phase, while legs 2, 4 and 6 just enter the transfer phase from the support phase. The duty ratio β_R is 0.5. The periodic functions of abductor joints in the legs 1 and 2 of virtual prototype can be set in the ADAMS software. The mathematical expressions are written as follows. Then

$$\begin{cases} y_{A_1} = \pi\theta_{1.3v_{\max}}^{(45^o,60^o)}\cos(bt)\Big/180 \\ y_{A_2} = -\pi\theta_{1.3v_{\max}}^{(45^o,60^o)}\cos(bt)\Big/180 \end{cases} \tag{51}$$

The period time T is assumed as 1 s. Based on (51), we can obtain that the value of b is 2π. According to Figures 13 and 14, the simulation verification of robot walking is carried out by the ADAMS software. The virtual simulation of robot walking is shown in Figure 21.

In Figure 19, it can be obtained that the walking speed of robot is about 1.3 $v_{\max}$. Based on the simulation data, we can conclude that the walking speed of virtual robot is the same as the target speed of real robot. The reasonable of maximum walking speed method is proved for the range of rotating speed of the abductor joint. Meanwhile, the range analyses of rotating speed of the hip joint and knee joint are effective.

VI. APPLICATIONS AND EXPERIMENTS

Based on the results of research, a prototype of an electrically driven large-load-ratio six-legged robot is developed. To more effectively validate the rationality of maximum walking speed method on the analysis of articulated rotating speed, the walking speed experiments of prototype are carried out by using 0.4 times the maximum walking speed as the goal speed. The ant-typed tripod gait is employed to perform the walking speed experiments of prototype. The duty ratio β_R is 0.5. Then, the movement time (TM) is set as 100 ms in the programmable multi-axis controller (PMAC). The support distances of the legs are set to 0.2 m in the support phase. Hence, the theoretical walking distance of prototype should be $2v_{\max}T/5$ in a gait period T. Figure 22 shows the walking experiments of the speed $2v_{\max}/5$ under the loads of 1519 N and 0 N. The climbing experiment of robot under the slope of 35° is also shown in Figure 22. Based on the range sensor installed in the body of robot, the walking distance l_{robot} of robot can be obtained with the change of time t. Then, the curves of walking speed are plotted and shown in Figure 23.

According to Figure 23, we can conclude that the curves of walking speed of the robot body are approximately consistent under the load of 1519 N and 0 N. Then, the comparative analysis is carried out between the actual walking speed of prototype and the theoretical walking speed $2v_{\max}/5$. The comparative results show that they are basically the same. Based on the data of articulated rotating speeds, we developed an electrically driven large-load-ratio six-legged robot. And the prototype of robot can successfully climb the slope of 35°. The phenomenon that the output speeds of joints do not meet the requirements of the actual working conditions does not appear. Hence, the reasonableness of proposed maximum walking speed method can be verified for the articulated rotating analysis of the large-load-ratio six-legged robot.

Based on Figures 11 and 22, we can conclude that the legs 1 and 2 can fully reflect the walking characteristics of the support phase and transfer phase when the large-load-ratio six-legged robot walks under the ant-type tripod gait. Then, the pulse numbers of servo motors for the abductor joints, hip joints, and knee joints of legs 1 and 2 are respectively gained based on the PMAC motion control card. Figure 24 plots the pulse number curves under the walking speed $2v_{\max}/5$. In Figure 24, the minus sign only indicates that the steering of servo motor is opposite to the specified positive steering.

According to the correspondence between the pulse numbers of servo motors in Figure 24 and rotating speeds of

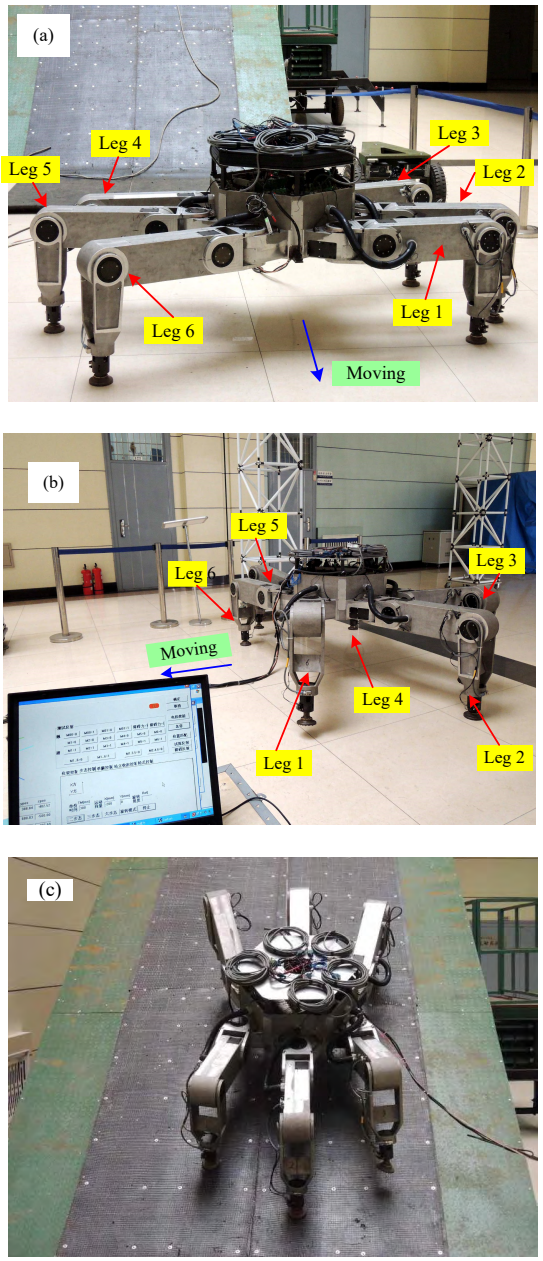

FIGURE 22. Walking experiments of the large-load-ratio six-legged robot: (a) walking experiment of speed 2 $v_{max}/5$ under the load of 1519 N, (b) walking experiment of speed 2 $v_{max}/5$ under the load of 0 N, and (c) walking experiment under the slope of 35°.

joints and the reduction ratios of articulated drives, the output rotating speeds of the abductor joints, hip joints, and knee joints of legs 1 and 2 can be gained. Then, the obtained output rotating speeds of joints are within the theoretical calculation ranges of articulated rotating speeds in Section IV. Hence, the walking experiment results of the electrically driven large-load-ratio six-legged robot show that the proposed method of articulated rotating speed analysis is reasonable and effective. The maximum walking speed method can be reliably applied to the development of the large-load-ratio multi-legged robots.

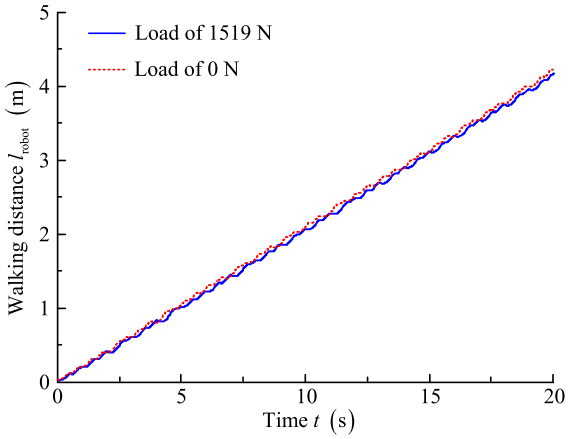

FIGURE 23. Curves of walking speed for robot body.

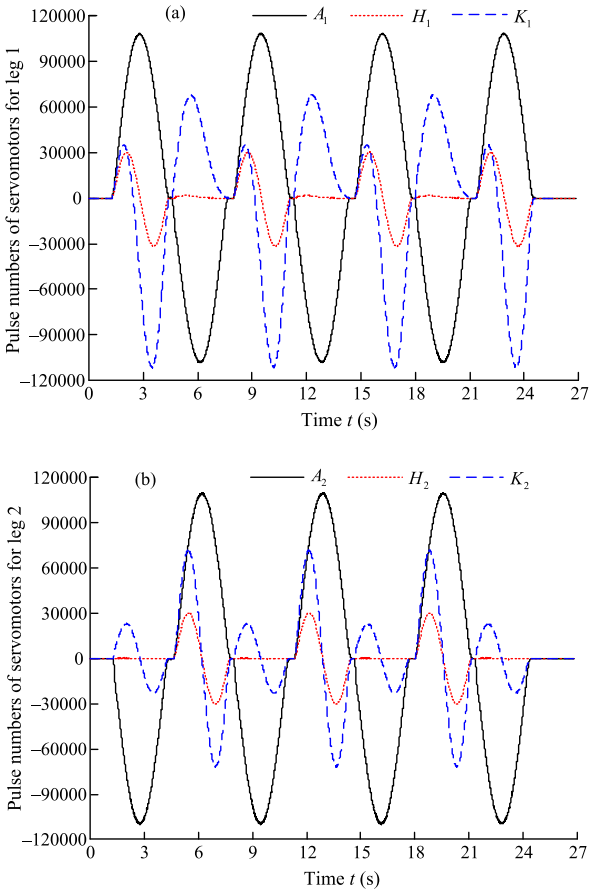

FIGURE 24. Pulse number curves of servo motors for legs 1 and 2: (a) leg 1 and (b) leg 2.

VII. CONCLUSIONS

To reasonably match the drive devices and actuating devices at the joints of the large-load-ratio multi-legged robots, this article presents the maximum walking speed method for quickly and accurately obtaining the range of articulated rotating speed by taking the electrically driven large-load-ratio six-legged robot as an example. Based on the structures of hexapod insects and the technical indicators of robot,

the body configuration of electrically driven large-load-ratio six-legged robot is constructed as a regular polygon. The walking leg is employed as the support leg of robot. The linkage proportion of single leg is determined as 9:25:25.

To prove the rapidity, accuracy, and conciseness of the maximum walking speed method, the analyses of the forward kinematics and inverse kinematics of robot are implemented based on the D–H method. Then, the range of rotating speed of the abductor joint is only effectively confirmed in a single leg. The ranges of rotating speeds of the hip joint and knee joint cannot be obtained Through rotating one of the joints to achieve the maximum speed index of robot, the maximum walking speed method is employed to establish the mathematical relationships between the articulated rotating angles and the maximum walking speed index of robot. The ranges of articulated rotation angles are obtained. The analysis results for the rotating speed of abductor joint are consistent between the D-H method and maximum walking speed method through the comparative analysis. The accuracy of the proposed maximum walking speed method is verified. Based on the rotation of a joint to achieve the maximum walking speed of robot, the output rotating speeds of the hip joint and knee joint at the minimum and maximum rotation angles are respectively obtained by the maximum walking speed method, when the robot walks under the crab-type tripod gait. The variation trends of the output rotating speed and rotating angle of abductor joint are also gained with the changes in the rotation angles of the hip joint and knee joint under the ant-type tripod gait.

The 3D model of virtual prototype is constructed and imported into ADAMS software. The simulation verification of robot walking is implemented. The simulation result shows that the walking speed of virtual robot is the same as the target speed of real robot. Based on results of research, an electrically driven large-load-ratio six-legged robot is developed. According to the prototype of robot, the walking experiments are executed. The velocity curves of the gravity center of bearing platform are respectively gained under the rated load and no load. The pulse number curves of articulated servo motors are also obtained under the rated load. The prototype of robot can successfully climb the slope of 35°. The walking experiment results of prototype show that the proposed maximum walking speed method is reasonable and effective and can be reliably applied to the development of the large-load-ratio multi-legged robots.

REFERENCES

[1] K. Nozaki and T. Murakami, "A motion control of two-wheels driven mobile manipulator for human-robot cooperative transportation," in *Proc. IECON*, Porto, Portugal, Nov. 2009, pp. 1574–1579.

[2] B. L. Luk, D. S. Cooke, S. Galt, A. A. Collie, and S. Chen, "Intelligent legged climbing service robot for remote maintenance applications in hazardous environments," *Robot. Auton. Syst.*, vol. 53, no. 2, pp. 142–152, Nov. 2005.

[3] B. H. Wilcox *et al.*, "ATHLETE: A cargo handling and manipulation robot for the moon," *J. Field Robot.*, vol. 24, no. 5, pp. 421–434, May 2007.

[4] M. Raibert, K. Blankespoor, G. Nelson, and R. Playter, "BigDog, the rough-terrain quadruped robot," in *Proc. 17th IFAC*, Seoul, South Korea, Jul. 2008, pp. 10822–10825.

[5] H. Zhuang, H. Gao, Z. Deng, L. Ding, and Z. Liu, "A review of heavy-duty legged robots," *Sci. China Technol. Sci.*, vol. 57, no. 2, pp. 298–314, Feb. 2014.

[6] B. Gassmann, F. Zacharias, J. M. Zöllner, and R. Dillmann, "Localization of walking robots," in *Proc. IEEE Int. Conf. Robot. Auton.*, Barcelona, Spain, Apr. 2005, pp. 1471–1476.

[7] M. S. Erden and K. Leblebicioğlu, "Free gait generation with reinforcement learning for a six-legged robot," *Robot. Auton. Syst.*, vol. 56, no. 3, pp. 199–212, Mar. 2008.

[8] K. Kurashige, T. Fukuda, and H. Hoshino, "Reusing primitive and acquired motion knowledge for gait generation of a six-legged robot using genetic programming," *J. Intell. Robot. Syst.*, vol. 38, pp. 121–134, Sep. 2003.

[9] S. Inagaki, H. Yuasa, and T. Arai, "CPG model for autonomous decentralized multi-legged robot system—Generation and transition of oscillation patterns and dynamics of oscillators," *Robot. Auton. Syst.*, vol. 44, nos. 3–4, pp. 171–179, Sep. 2003.

[10] B. L. Luk, S. Galt, and S. Chen, "Using genetic algorithms to establish efficient walking gaits for an eight-legged robot," *Int. J. Syst. Sci.*, vol. 32, no. 6, pp. 703–713, Jun. 2001.

[11] A. Irawan and K. Nonami, "Optimal impedance control based on body inertia for a hydraulically driven hexapod robot walking on uneven and extremely soft terrain," *J. Field Robot.*, vol. 28, no. 5, pp. 690–713, Sep./Oct. 2011.

[12] Y. Zhao, X. Chai, F. Gao, and C. K. Qi, "Obstacle avoidance and motion planning scheme for a hexapod robot Octopus-III," *Robot. Auton. Syst.*, vol. 103, pp. 199–212, Mar. 2018.

[13] P. E. Mendez-Monroy, "Walking motion generation and neuro-fuzzy control with push recovery for humanoid robot," *Int. J. Comput. Commun.*, vol. 12, no. 3, pp. 330–346, Jun. 2017.

[14] Y. Tian and F. Gao, "Efficient motion generation for a six-legged robot walking on irregular terrain via integrated foothold selection and optimization-based whole-body planning," *Robotica*, vol. 36, no. 3, pp. 333–352, Mar. 2018.

[15] A. Martinez, B. Lawson, and M. Goldfarb, "A controller for guiding leg movement during overground walking with a lower limb exoskeleton," *IEEE Trans. Robot.*, vol. 34, no. 1, pp. 183–193, Feb. 2018.

[16] X. Xiong, F. Wörgötter, and P. Manoonpong, "Neuromechanical control for hexapedal robot walking on challenging surfaces and surface classification," *Robot. Auton. Syst.*, vol. 62, pp. 1777–1789, Dec. 2014.

[17] M. M. Gor, P. M. Pathak, A. K. Samantaray, J. M. Yang, and S. W. Kwak, "Control of compliant legged quadruped robots in the workspace," *Simulation*, vol. 91, no. 2, pp. 103–125, Feb. 2015.

[18] J. E. Pratt and R. Tedrake, "Velocity-based stability margins for fast bipedal walking," in *Fast Motions in Biomechanics and Robotics* (Lecture Notes in Control and Information Sciences), vol. 340. Berlin, Germany: Springer, 2006, pp. 299–324.

[19] X. Wang, M. Li, W. Guo, P. Wang, and L. Sun, "Velocity control of a bounding quadruped via energy control and vestibular reflexes," *J. Bionic Eng.*, vol. 11, no. 4, pp. 556–571, Oct. 2014.

[20] T. Zhang, H. An, and H. Ma, "Joint torque and velocity optimization for a redundant leg of quadruped robot," *Int. J. Adv. Robot. Syst.*, vol. 14, no. 5, pp. 1–12, Sep. 2017.

[21] X. Zhang, E. Mingcheng, X. Zeng, and H. Zheng, "Adaptive walking of a quadrupedal robot based on layered biological reflexes," *Chin. J. Mech. Eng.*, vol. 25, no. 4, pp. 654–664, Jul. 2012.

[22] K. J. Waldron and R. B. McGhee, "The adaptive suspension vehicle," *IEEE Control Syst. Mag.*, vol. 6, no. 6, pp. 7–12, Dec. 1986.

[23] D. V. Lee and A. A. Biewener, "BigDog-Inspired studies in the locomotion of goats and dogs," *Integr. Comp. Biol.*, vol. 51, no. 1, pp. 190–202, Jul. 2011.

[24] E. Krotkov and R. Simmons, "Perception, planning, and control for autonomous walking with the Ambler planetary rover," *Int. J. Robot. Res.*, vol. 15, no. 2, pp. 155–180, Apr. 1996.

[25] J. E. Bares and D. S. Wettergreen, "Dante II: Technical description, results, and lessons learned," *Int. J. Robot. Res.*, vol. 18, no. 7, pp. 621–649, Jul. 1999.

[26] A. Irawan and K. Nonami, "Compliant walking control for hydraulic driven hexapod robot on rough terrain," *J. Robot. Mechatron*, vol. 23, no. 1, pp. 149–162, Feb. 2011.

[27] J. J. Craig, "Forward Kinematics," in *Introduction to Robotics: Mechanics and Control*, 4th ed. New York, NY, USA: Pearson, 2017, pp. 32–55.

[28] T.-T. Lee, C.-M. Liao, and T. K. Chen, "On the stability properties of hexapod tripod gait," *IEEE J. Robot. Autom.*, vol. 4, no. 4, pp. 427–434, Aug. 1988.
[29] P. Ramdya *et al.*, "Climbing favours the tripod gait over alternative faster insect gaits," *Nature Commun.*, vol. 8, Feb. 2017, Art. no. 14494.
[30] S. Miao and D. Howard, "Optimal tripod turning gait generation for hexapod walking machines," *Robotica*, vol. 18, pp. 639–649, Nov./Dec. 2000.

HONGCHAO ZHUANG received the master's degree from Yanshan University, China, in 2010, and the Ph.D. degree from the Harbin Institute of Technology, China, in 2015. He is currently a Lecturer with the College of Mechanical Engineering, Tianjin University of Technology and Education, China. His research interests include special robotics, aerospace mechanism and control, mechanics, and control and simulation of mobile robots.

NING WANG received the master's and Ph.D. degrees from Yanshan University, China, in 2010 and 2015, respectively. She is currently a Lecturer with the College of Information Technology Engineering, Tianjin University of Technology and Education, China. Her research interests include motion planning and control, and simulation of legged robots.

HAIBO GAO received the Ph.D. degree in mechanical engineering from the Harbin Institute of Technology, China, in 2003, where he is currently a Professor and a Supervisor for Ph.D. candidates with the State Key Laboratory of Robotics and System. His research interests include aerospace mechanism and control, and rover movement state estimation.

ZONGQUAN DENG received the master's degree from the Harbin Institute of Technology, China, in 1984. He is currently an Academician of the Chinese Academy of Engineering, a Professor, and a Supervisor for Ph.D. candidates with the State Key Laboratory of Robotics and System, Harbin Institute of Technology. His research interests include special robotics, planetary rover technology, and aerospace mechanisms and control.